MASTER

A numerical human lower leg model for injury prediction development, evaluation and application

van Rooij, L.

Award date:
2001

A Numerical Human Lower Leg Model for Injury Prediction

Development, Evaluation and Application

WFW-report 2001.15 L. van Rooij

Master's Thesis, April 2001

Examination Board:

Prof. Dr. H. Nijmeijer	(TUE)
Prof. Dr. Ir. J.S.H.M. Wismans	(TNO/TUE)
Dr. Ir. P.H.M. Bovendeerd	(TUE)
Dr. Ir. N. van de Wouw	(TUE)
Ir. H.J. Cappon	(TNO)

Eindhoven University of Technology
Faculty of Mechanical Engineering
Eindhoven, The Netherlands

TNO Automotive
Crash Safety Centre
Delft, The Netherlands

Samenvatting

De introductie van veiligheidsvoorzieningen in auto's, zoals gordels en airbags, heeft tot een afname van het aantal dodelijke verkeersslachtoffers geleid. Daardoor zijn minder levensbedreigende letsels van groter belang geworden, waaronder ook onderbeen-, enkel- en voetletsels. Deze letsels resulteren vaak in langdurige revalidatie en hoge economische kosten. Er zijn veel modellen ontwikkeld die de kinematica van het onderbeen bij impact beschrijven, echter tot nu toe is er geen model dat gebruikt kan worden om letsels te voorspellen.

Het doel van dit onderzoek bestaat uit het ontwikkelen van een numeriek mensmodel van het onderbeen, dat ten eerste een correcte globale kinematica beschrijft voor impact op de voet van de inzittende als gevolg van een frontale botsing en dat ten tweede letsels kan voorspellen gebaseerd op lokale effecten, zoals krachtdoorleiding en spanningen. Het model moet geëvalueerd worden aan de hand van experimentele data en aan de hand van gegevens uit bestaande ongevallen databases.

Uit literatuurstudie naar bestaande ongevallen kunnen drie belangrijke letsel mechanismen onderscheiden worden; axiale impact, dorsiflexie en inversie of eversie. Daarnaast is de anatomie van het onderbeen bekeken, om de correcte geometrie van de verschillende weefsels, zoals bot, kraakbeen, ligamenten, spieren, vet en huid te kunnen implementeren. Het mechanisch gedrag van deze weefsels is onderzocht om later te transformeren in constitutieve materiaalwetten.

Het onderbeen model is van een gecombineerd eindige elementen en multibody type. De botten van onderbeen, enkel en hiel van de voet zijn weergegeven door een eindige elementen mesh van shell en solid elementen, met lineair elastoplastisch materiaalgedrag. Deze beschrijving kan botdeformatie simuleren en geeft lokale data weer, zoals krachten en spanningen. De voorvoet bestaat uit starre lichamen, onderling verbonden door kinematische gewrichten. Contact tussen botdelen wordt gerealiseerd door een contact algoritme dat ook het mechanisch gedrag van kraakbeen meeneemt. Ligamenten zijn geïmplementeerd als niet-lineaire veren met voorspanning en hysteresis. Spieren hebben een passieve stijfheid en kunnen actief samentrekken. Het vet- en huidweefsel op de voetzool wordt beschreven door een solid mesh met lineair elastich materiaalgedrag met hysteresis.

Het model is geëvalueerd aan de hand van vijf kadaverexperimenten, uitgevoerd bij het Automobile Safety Laboratory van de University of Virginia. Bij drie experimenten traden botbreuken op en bij twee experimenten was de Achilles pees voorgespannen. De globale kinematica en axiale krachten correleren goed met de experimenten, terwijl andere signalen te veel verstoord worden door onbekende randvoorwaarden van de experimenten of door niet-fysische trillingen in de simulaties. Data van het Transport Research Laboratory zijn gebruikt voor

evaluatie van het model voor lagere impactsnelheid. Een goede correlatie is gevonden voor de versnellingsrespons en de dorsiflexie hoek.

Om letsels te voorspellen zijn gegevens nodig op een lokaal niveau. De eindige elementen mesh geeft externe knooppuntskrachten en elementspanningen weer. De verdeling van de externe knooppuntskrachten over de botdelen laat zien dat in simulaties de krachten door de gewrichtsoppervlakken geleid worden. Een correcte verandering van krachtdoorleiding wordt weergegeven voor inversie en eversie simulaties, echter bij dorsiflexie tests zijn de veranderingen slechts klein. De spanningverdeling over de mesh van de botdelen laat grote onregelmatigheden zien, veroorzaakt door de grofheid van de mesh. Dit maakt het onmogelijk om hieruit conclusies te trekken. Desalniettemin blijkt de vloeispanning goed letsels te kunnen voorspellen, gezien de gevonden correlatie tussen model en experimenten. Geen conclusies kunnen getrokken worden uit het gedrag na breuk.

Verder blijkt uit een parametergevoeligheidsstudie dat er verder onderzoek plaats moet vinden naar de niet-fysische trillingen en dat de parameters van het eindige elementen model niet noodzakelijk overeenkomen met de referentiewaarden door de grote vereenvoudiging, terwijl multibody parameters binnen hun biofidelity bereik blijven.

Summary

Since the introduction of car safety restraint systems, like belts and airbags, the number of traffic deaths decreased seriously. This increased the importance of less life-threatening injuries, like those inflicted to the lower leg. Lower leg injuries often result in long term impairment and high economic costs. Many models have been developed that simulate lower leg kinematics under impact conditions, but so far no model can be used for injury prediction purposes.

The aim of this study is to develop a numerical human lower leg that shows correct global kinematic behaviour under car occupant frontal impact conditions and which can predict injuries based on locally observed data, like load path force and stress. The model needs evaluation against experimental and real world accident data.

A study of real world accident databases proved that three injury mechanisms of major importance can be distinguished; axial impact, dorsiflexion and inversion or eversion. Furthermore the anatomy of the lower leg is investigated in order to be able to implement the correct geometry of different tissues like bone, cartilage, ligaments, tendons, muscles, fat and skin. The mechanical behaviour of the different tissues is investigated in order to be transformed into constitutive material laws.

The lower leg model is of a combined finite element and multibody approach. The bones of lower leg and hind foot are composed of a finite element mesh of both shell and solid elements, with linear elastoplastic material behaviour. This description simulates bone deformation and provides local information on force and stress. The forefoot consists of rigid bodies connected by kinematic joints. Contact between bone parts is realised by a contact algorithm that accounts for cartilage behaviour. Ligaments are implemented as non-linear springs with initial pretension and hysteresis and muscles exhibit a passive stiffness and allow for active muscle behaviour. Plantar tissue is implemented in a finite element solid mesh, with linear elastic material behaviour with hysteresis.

The model is evaluated against a series of five high severity PMHS experiments obtained from the Automobile Safety Laboratory of the University of Virginia. In three experiments failure of bone parts occurred, while in two experiments Achilles pretension was applied. Global kinematics and axial forces show good correlation with the experiments, other signals are too much dependent on unknown boundary conditions or show non-physical vibrations. Test data from the Transport Research Laboratory are used for low severity evaluation of the model, where good correspondence shows for acceleration response and dorsiflexion angle.

For injury prediction purposes, information is needed on a local level. The finite element mesh provides external nodal forces and element stresses. The distribution of external nodal forces shows that the loads in axial impact simulations are

transferred through the articular surfaces of the bone parts. A correct change of load path is shown for both inversion and eversion simulations, while in the dorsiflexion simulation less changes appear. The stress distribution over the bone mesh shows large irregularities, caused by mesh coarseness. It is therefore impossible to draw conclusions from provided stress information. Nevertheless the yield stress is shown to be a good predictor for injuries, since failure correlation is found for UVa experiments. No post-failure behaviour is modelled in the current model.

Furthermore a parameters sensitivity study points out that the non-physical vibrations need further investigation, and that the finite element parameters do not necessarily correspond to reference values found in literature, whereas multibody parameters stay within their biofidelity ranges.

Contents

1 Introduction 1
1.1 Context 1
1.2 Objectives 2
1.3 History of Human Lower Leg Models 2
1.4 Requirements 4
1.5 Outline 5

2 Anatomy of the Human Lower Leg 7
2.1 Bone 7
2.1.1 Bone Types and Microstructure 7
2.1.2 Bones of the Lower Leg 8
2.1.3 Cartilage 9
2.2 Ligaments and Tendons 9
2.3 Muscles 11
2.4 Plantar Tissue 12

3 Injuries, Injury Mechanisms and Tolerances 13
3.1 Injury Statistics 13
3.2 Injury Mechanisms 15
3.2.1 Influence of Inertial Loading 16
3.2.2 Concluding Remarks 17
3.3 Injury Tolerances 17

4 Material Characterisation 18
4.1 Bone 18
4.1.1 Cortical Bone 18
4.1.2 Trabecular bone 19
4.1.3 Model parameters 19
4.2 Ligaments and Tendons 19
4.3 Muscles 20
4.4 Plantar Tissue 21

5 The Adult Lower Leg Model 23
5.1 Geometry 23
5.2 Bone system 23
5.2.1 Inertial Properties 24
5.2.2 Finite Element Modelling 25
5.2.3 Multibody Modelling 26
5.3 Ligaments 27
5.4 Muscles 28
5.5 Plantar Tissue 28
5.6 Contact Description 28

6 Evaluation of the Adult Lower Leg Model 31
6.1 UVa Tests 31
6.1.1 Experimental UVa Test Setup 31
6.1.2 Modelling Of UVa Test Setup 32
6.1.3 Results of UVa Tests 34
6.2 TRL Tests 37
6.2.1 Experimental TRL Test Setup 37
6.2.2 Modelling of TRL Test Setup 37
6.2.3 Results of TRL Tests 38

7 Parameter Sensitivity Study 39
7.1 Bone Properties 39
7.2 Cartilage Contact 39
7.3 Ligaments 40
7.4 Plantar Tissue 40
7.5 Vibrations 41

8 Injury Prediction 42
8.1 Injury Parameters 42
8.2 Load Paths 43
8.3 Correlation with Injury Mechanisms 44
8.3.1 Axial Impact 44
8.3.2 Dorsiflexion 45
8.3.3 Inversion and Eversion 46

9 Discussion 48
9.1 Model Evaluation 48
9.2 Parameter Sensitivity 50
9.3 Injury Prediction 50

10 Conclusions and Recommendations 53

References 56

Appendix A Injury Statistics A-1

Appendix B Material Properties B-1

Appendix C Geometry Properties C-1

Appendix D UVa Test Setup D-1

Appendix E UVa Results E-1

Appendix F TRL Results F-1

1 Introduction

This report constitutes towards the master's degree project at Eindhoven University of Technology. The project is carried out within the section of Biomechanics at TNO Automotive, Crash Safety Centre in co-operation with the section of Engineering Dynamics and Biomechanics of the department of Mechanical Engineering of Eindhoven University of Technology. This study complies with the aim of TNO to improve automobile safety, by the development of a numerical human lower leg model under impact conditions.

1.1 Context

In the late 1960's the number of traffic accidents with lethal or severe injury consequences increased enormously due to intensified traffic and faster cars. This statistical increase led to awareness of governments, consumer organisations and car manufacturers of the importance of legislation concerning traffic safety, both passive and active. A decrease in traffic deaths and severe injuries was attained in 1971 when the seat belt was introduced. The introduction of airbag systems in the 1980's contributed to a further decrease. Both restraint systems are mainly designed to reduce head and neck injuries. This led to an increase of relative importance of injuries to other body parts, like the lower extremities. Although mostly not life-threatening, injuries to the lower extremities result in long term impairment and high economic costs. This increased relative importance has caused a shift of focus towards lower extremity injuries.

Presently the primary tools used for injury assessment are mechanical dummies. These mechanical human surrogates are able to withstand full-scale crash tests while simultaneously measuring a number of signals. Thus information is provided on global responses of the dummy in terms of accelerations, forces and moments in different body parts. In order to save costs in the design process, mathematical dummy models are used that constitute similar behaviour to mechanical dummies, but which can be used in a simulation environment.

Crash test dummies, both mechanical and mathematical, lack a biofidelic response in some accounts. At first the mechanical behaviour of steel, rubber and foam in a non-destructive structure can never correctly simulate the behaviour of soft tissues, fragile bones and active muscle behaviour. Secondly, the measured signals only provide global information on responses, thus lacking information on local phenomena like stresses and strains that in turn enable injury prediction.

Mathematical human body models are proposed as a possible solution to biofidelity requirements. In a simulation environment all tissue characteristics can be adopted in different material models. The geometry and kinematics of the model are not restricted to the engineering limitations that mechanical dummies contain.

Furthermore restrictions to dummy loadcells disappear, thus allowing the output of measured data in all areas of interest.

At TNO Automotive, Crash Safety Centre a research project on lower limb injuries started. This project involves the development of a mathematical human lower leg that can be used as a design tool for car manufacturers. This thesis contributes to the development of the mathematical human lower leg as it functions as a research tool for the prediction of injury mechanisms resulting from frontal impact with the aid of finite element modelling techniques, contact definitions and soft tissue constraints.

1.2 Objectives

The main objective of this research is to develop a model of a human lower leg that predicts injuries occurring due to contact with the car interior under frontal crash impact conditions. Injury prediction is considered important for three mechanisms occurring in real life traffic accidents: compressive loading, dorsiflexion and inversion/eversion of the foot. Local injury prediction requires a detailed model that provides information on load paths and local effects, like stresses and strains. A correlation should be found between injuries occurring in experiments and stress concentrations at corresponding locations.

1.3 History of Human Lower Leg Models

The first numerical simulations involved the lower leg model of the Hybrid III dummy. The dummy lower leg consists of an ankle joint, with three rotational degrees of freedom and accompanying rotational stiffness. The tibia model consists of a steel bar, with two integrated load cells. Nowadays, the Hybrid III dummy lower leg and its models are considered not to be biofidelic. New dummy models are proposed [Artis, 2000].

The lack of biofidelity of dummy models instigated the development of human lower leg models. These models are designed to represent human anatomy, kinematics and biomechanics more accurately than steel, rubber and foam of dummy models. Material behaviour of bone, ligaments, flesh and skin are implemented. It is even possible to implement active muscle behaviour.

Muriel Beaugonin [Beaugonin, 1995] of ESI was the first to develop a finite element model of the human ankle/foot-complex. It consisted of 1872 shell elements and 788 solid elements. Bone materials are implemented as rigid shell elements; soft tissue is implemented as deformable membrane elements, whereas the ligaments of the foot are modelled with deformable bars. The influence of non-linear, anisotropic material behaviour with hysteresis for soft tissue was found to be small [Beaugonin, 1996 [1]]. From inversion/eversion simulations [Beaugonin, 1996 [2]] it was concluded that pretensioning of the Achilles tendon did not influence the response at high-energy impacts. The use of linear elastic bone

behaviour was found to correlate better with cadaveric dorsiflexion tests, than rigid bone does [Beaugonin, 1997]. A possible explanation for this divergence is the energy absorbed by deformable bones. No conclusions on a local level are drawn from the detailed finite element modelling of bone. The boundary conditions of the model raise doubts about the biofidelity of the simulation. The foot is fixed by screwing calcaneus and phalanxes to the footplate and tibia and fibula are constrained at approximately eight centimetres above the ankle joint. The model thus does not implement plantar soft tissue behaviour and tibia and fibula deformations are ignored. In addition, the fixation restrains kinematics, which does not occur in real world crashes.

A similar model of the human foot/ankle complex [Tannous, 1996] is reported to be promising for the purpose of predicting injuries and the development of an enhanced ankle injury criterion. The anatomical structure and ligamentous properties are responsible for the capacity to replicate the dynamic response. The model is evaluated with a limited set of data and finite element properties are reported to be insufficient for injury prediction purposes. An attempt to develop a FE ankle/foot model using CT scan data was made [Beillas, 1999] in order to be able to simulate joint kinematics resulting from geometrical properties and biomechanical restraints. Improvements to the model would be the modelling of bone as finite elements in order to draw conclusions from local data like stresses and strains. Another finite element model of the lower leg was developed and validated against static bending, quasi-static rotations and impact loading to the foot [Furusu, 1999]. All joint articulations are defined by spherical joints, thus inadequately describing force transmission through bones.

The development of a global human leg model in MADYMO was ignited by Chantal Parenteau [Parenteau, 1996[1]]. The model was fully based on multibody dynamics. It comprises rigid bodies for tibia, malleoli, talus, calcaneus, tarsals and forefoot. Three joints determine the kinematics of the model: the ankle joint, subtalar joint and midtarsal joint. Injury criteria for eversion and inversion are implemented by two free joints in the malleoli, that are initially locked and will be unlocked at predetermined failure thresholds in ankle joint rotations. Also rotational failure limits for dorsiflexion and plantarflexion are implemented. The model is validated for quasi-static loading, but it can be used for injury prediction since failure angles are found to be independent of moments and forces. Recommendations for further development of the model are an investigation on the influence of bracing on lower leg injury mechanisms. The model was further improved in order to be able to predict injuries resulting from oblique plantar impact [Hall, 1998]. In addition the model was extended to upper leg and pelvis. Geometry, inertial and mass properties were determined from CT scans. The locations, degrees of freedom and stiffness of the joints are lumped in kinematic constraints with experimentally observed parameters. The mechanical properties of the eight major ankle ligaments are represented in a quasi-linear viscoelastic element [Fung, 1981] parallel with a non-linear elastic spring element. Failure is incorporated in experimentally determined maximum values for tensile force. The

passive stiffness of the triceps surae muscle is implemented in non-linear elastic elements and an experimentally determined value for Achilles rupture is used. The model is validated for two impact scenarios and predicts peak tibia compression, ankle motion and Achilles tension. A further improvement of the multibody model of the human lower extremity consists of an implementation of active musculature and the application of improved fracture models [Cappon, 1999]. The upper leg part is adopted from the Hybrid III dummy model. Through the whole lower extremity musculature is implemented exhibiting Hill muscle behaviour, including a passive and active stiffness. Fracture mechanisms are implemented in the unlocking of kinematic constraints when reported injury tolerance levels were attained for a duration of 1 millisecond. Injury tolerances used were 45° ankle dorsiflexion, 60 Nm tibia torque and 7.8 kN tibia compressive force. This global response of the model is extendedly validated against PMHS, aware and unaware volunteer toe and heel impact tests. The model proved to be applicable for injury prediction, where global signals exceed the experimentally defined injury tolerances, e.g. maximum tibia compression force and ankle rotation fracture limits. Furthermore it allows drawing conclusions on the effects of bracing on injuries. Currently this model is being updated with more ligaments and muscles and a better anatomical description instead of the former used ellipsoid shapes.

From this global overview of existing models it can be concluded that so far no model that is validated against various impact conditions, allows for local injury prediction. The deformable bone models have so far only been used for studying effects of energy absorbence by elastic bone, whereas finite element formulations can provide information on local stresses and strains. Other models suffer from kinematic assumptions that do not contribute to the prediction of injuries, but merely simulate the experimentally observed injury tolerances. This induces the need for a model that fulfils the objectives stated above.

1.4 Requirements

The development of a mathematical model derived from real world and experimental observations incorporates a number of assumptions. In order to justify these modelling assumptions the following points should be considered:

- The development of the model should be based on experimentally observed characteristics. Parameters necessary for defining the human lower leg in a mathematical code should lie within the ranges defined by different investigations under comparable circumstances, as found in literature references. Also different components of the model need evaluation on a local level in order to justify the response of the model as an assembly of components;

- In the development of the model attention should be given to the appropriate method of modelling. The mathematical code allows for both finite element and multibody techniques. Both methods have their advantages and

disadvantages. Finite element structures allow for elastic and plastic deformation and provide information on stresses and strains. Multibody techniques allow for non-linear material behaviour lumped in a kinematic description with low computational time. A justification of the use of either technique is an integral part of the model description;

- The model needs evaluation of the global response to impact loading. The mechanical behaviour of the model under impact loading conditions should show close resemblance with a number of different experiments executed. All boundary conditions of the experimental setup should be considered, as well as the limitations to the biofidelity of these experiments;

- A sensitivity analysis with various parameters should be executed. A validated response may very well be obtained by tuning one parameter. However, the validity of the variation of this one parameter carries uncertainty, due to the complexity of the model. In order to justify the response of the model the influence of a variety of parameters needs investigation. Also a large spread in human characteristics or anthropometry is apparent under car occupants in real life. The influence of this wide range on the response has to be investigated in order to justify the use of just one 50^{th} percentile model;

- Load paths from impactor to knee should be constructed. This evokes the need for a detailed model, based on an anatomical description. The amount of modelling constraints should be reduced to the minimum in order to obtain a biofidelic response at all levels of modelling, global and detailed. Besides the previously discussed global response also the response on a smaller scale should be evaluated. This leads to the transmittance of forces through different load paths instead of the transmittance through a single kinematic joint.

1.5 Outline

Derived from this introduction, the outline of this thesis globally follows the requirements stated above. In the second chapter a description of the anatomy of the human lower leg determines the role various tissues play in the kinematics and response of the lower leg upon impact. The microstructure of different tissues allows for the justification of the use of certain material models, while the macrostructure determines the kinematic behaviour of the lower leg.

Chapter 3 is merely a literature survey on the occurrence of injuries in real world accidents. This chapter functions as a justification of this research, since it shows the increased relative importance of lower leg injuries. Furthermore it shows which bone parts are statistically most often injured and what injury mechanisms occur. Also an overview is given on experimentally observed injury tolerances and existing injury criteria.

In chapter 4 the characterisation of different materials is described. The provided structural information on tissues is transformed into mathematical descriptions. The mathematical descriptions or material models are described by parameters, of which reference values are reported.

The development of the adult lower leg model is described in chapter 5. Geometry and inertial properties are defined here. Also the decision process on the use of multibody or finite element descriptions for various structures is outlined in this chapter. Furthermore other modelling constraints are presented here, as there are cartilage, ligaments, muscles and plantar tissue.

The global response of the model is evaluated in chapter 6. A description of experiments executed is followed by the modelling of the experimental test setup. This leads to a presentation of the results considering all boundary conditions.

The sensitivity of the model to a variety of parameters in discussed in chapter 7. An explanation is given on chosen parameters and their influence on the model response.

The application of the developed model, injury prediction, is evaluated in chapter 8. First a number of parameters indicating injuries are defined, followed by an indication of load paths through the bones and correlations found between simulations, real world accidents and experiments.

The discussion that follows from the developed model, its evaluation and its application is presented in chapter 9, followed by conclusions and recommendations for further research in chapter 10.

2 Anatomy of the Human Lower Leg

In literature, the human lower limb is referred to as the leg, stretching from toes to thighs. Often the pelvis is included in human lower limb models and experiments. This study concentrates on the lower part of the lower limb, defined here as the leg from the knee joint down to the toes. The anatomy of the upper part is considered irrelevant here and will not be discussed any further.

The lower leg, as treated in this thesis, can be subdivided in three regions that differ both in structure and in function: the foot, the ankle and the leg. The foot is the horizontally orientated structure that provides stability to the human body. The ankle is merely a joint that enables most movements of the foot relative to the leg. The lower leg is a long load-bearing structure that exhibits active muscle behaviour.

The main constituents of the lower limb from a structural and mechanical point of view are bones, ligaments, muscles, fat and skin. All materials provide a different function, accompanying different mechanical behaviour. The anatomy, structural and mechanical behaviour of all materials will be discussed in the following paragraphs.

2.1 Bone

The skeleton is the main load bearing structure in the human body. All bones are stiff structures, interconnected by articulating joints.

2.1.1 Bone Types and Microstructure

Generally two types of bone are distinguished: long bones and short bones. Long bones are the bones that have uniaxial orientation. The only long bones in the lower leg are tibia and fibula. The extremities of the long bones are referred to as epiphysis. The outside layer (1 mm to 5 mm in thickness) of the epiphysis consists of cortical bone, also called compact bone. Cortical bone is a dense type of bone tissue, which is known for its high compression stiffness, its relatively isotropic material behaviour and Haversian systems [Fung, 1981]. On the outside surface of the epiphysis the articular joint surface is formed, which will be discussed later. The inside of the epiphysis is made up of trabecular bone, also called spongy bone. Its name derives from its appearance; small beams of bone form a network of bone with many cavities. The result is a low density, reduced stiffness tissue type. Nevertheless the beam system is known to have smart remodelling mechanisms to fulfil the demand for directional stiffness [Mullender, 1997]. Strong anisotropic stiffness can be achieved controlled by the loading path through the bone. The corpus of long bones, the diaphysis, comprises an outer layer of compact bone and an inside system of bone marrow. Bone marrow is responsible for the production of red blood cells, but no definite mechanical behaviour is attributed to it.

Short bones of different dimensions can be found in the foot. Calcaneus and talus are the largest and situated in the hindfoot. The forefoot comprises tarsals, metatarsals and phalanxes. All short bones exhibit the same properties as the epiphysis of long bones. The outside layer consists of compact bone, while the inside consists of trabecular bone. Also here articulated joint surfaces are formed, often different oddly curved surfaces, due to the complex kinematics of the foot.

Although different types of bone exist, bone as a tissue on a microstructural level appears approximately the same throughout. It is composed of a small percentage by volume of osteocytes, or bone cells. The major part of bone tissue is made up of intercellular substance, which in its turn is a composition of minerals and collagenous fibrils. The minerals provide density and compression stiffness, while the collagen provides elasticity and tensile stiffness to the bone tissue.

2.1.2 Bones of the Lower Leg

This paragraph discusses the bones of the lower leg from a structural point of view. The skeleton is composed of different long and short bones. Below the different bones will be discussed subsequently from proximal to distal end of the lower leg.

From a functional point of view, the tibia (see Figure 2.1) is the load bearing structure of the lower leg. At the proximal epiphysis it connects to the femur to form the knee joint. At the distal epiphysis it connects to the medial side of the talus. The articular surface of the tibia-talus connection is mainly horizontally oriented to transmit longitudinal forces. On the medial side of the tibia a 'knuckle' is formed, called medial malleolus. The malleolus functions as a constraint for lateral-medial displacement and rotation around the sagittal axis. The distal part of the tibia, just above the malleolus, is referred to as ankle pilon in crash injury literature references.

Figure 2.1: bone structures of the lower leg

The fibula functions merely as a force transmitter for rotational movement of the foot relative to the leg. Its reduced diameter does not allow for severe axial loading. It does not exhibit a large horizontally oriented joint surface at the ankle joint, like the tibia does. The distal fibula does exhibit an extension, running down the talus on the lateral side. This lateral malleolus' function is assumed the same as the medial malleolus described above.

The talus connects to the leg by means of the ankle joint. Downward force transmittance to the foot occurs by two joint surfaces, one for axial loading to the calcaneus and one for connecting to the forefoot, in contact with the navicular bone, as Figure 2.2 shows. The calcaneus or heel bone connects at the subtalar joint

through three articular surfaces: anterior, medial and posterior. These three surfaces are defined by the geometry of both talus and calcaneus. The connection of the calcaneus to the forefoot is realised by the cuboid bone. The imaginary joint between talus and calcaneus in the hindfoot and cuboid and navicular bone in the forefoot is often called Chopart's joint. On the medial side of the foot three small bones stretch forward: medial, intermediate and lateral cuneiform bones.

The further extension to the forefoot is realised by Lisfranc's joint. This imaginary joint connects cuboid and cuneiforms to five metatarsals. The metatarsals in their turn connect to phalanxes. The phalanxes consist of two or three bones in each of the five branches that form the toes.

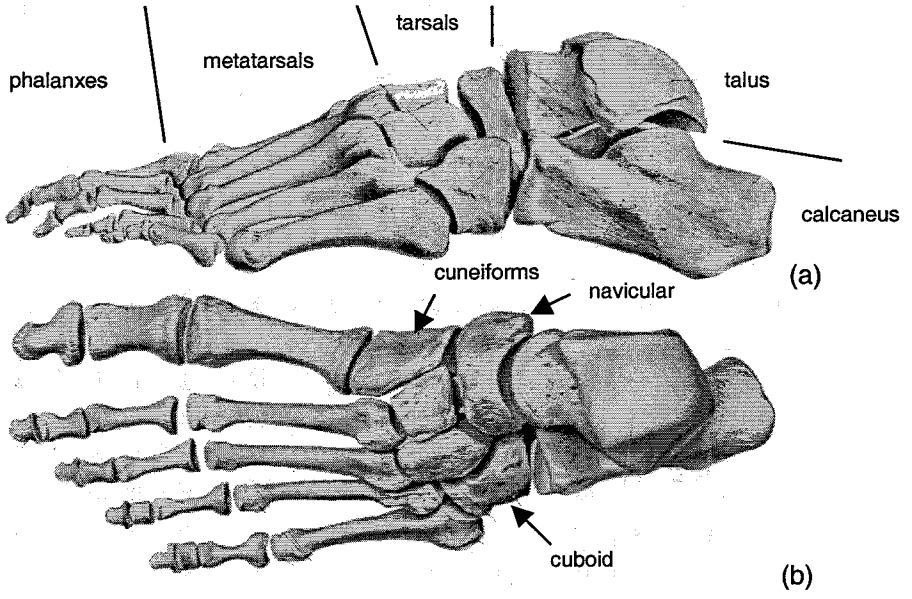

Figure 2.2: bone structures of the left foot in lateral (a) and proximal (b) view

2.1.3 Cartilage

As stated before joint surfaces of bones are covered with a layer of cartilage. The cartilage layer functions as a low friction sliding surface and it absorbs and dissipates the forces exerted on it. The dissipative behaviour is a result of the composition of the intercellular substance of cartilage tissue. This substance - produced by chondrocytes - consists of collagen, water and proteoglycans. The collagen fibrils form a network that is surrounded by the proteoglycans and water. The proteoglycans have negative charged side chains that draw water into the network. As a result, cartilage is a gel-like tissue.

2.2 Ligaments and Tendons

The collection of ligaments in the human body function as a constraint for the skeletal system. Ligaments interconnect bones, thus restraining relative movements. Tendons also restrain the locomotive system and they also function as intermediates for bone and muscles.

The composition of ligament and tendon tissue is adapted for their mechanical function. Fibrocytes are surrounded by an intercellular substance, composed of reticulinar, collagen and elastin fibres and a base substance. The mechanical behaviour is mainly attributed to collagen and elastin fibres. The collagen fibres are unidirectionally orientated in the longitudinal direction of the joint. If the ligament is untensioned the collagen fibres are in a curved state. Surrounding the collagen fibres is a network of elastin fibres, providing the tissue with elasticity.

The two most important joints in the lower leg are knee and ankle joint. Both joints are encapsulated by a number of ligaments. Since the biomechanical behaviour of the knee joint is out of the scope of this thesis it will not be further discussed here. The ankle joint connects tibia, fibula, talus and calcaneus bones. Soft tissue restraints can be subdivided in a number of eight ligaments, as shown in Figure 2.3b and c. On the medial side of the ankle a number of three ligaments together form the deltoid ligament: tibiocalcaneal (1b), posterior tibiotalar (1c) and anterior tibiotalar ligament (1a). On the lateral side the remaining five ligaments are: anterior talofibular (2), posterior talofibular (3), calcaneofibular (4), anterior tibiofibular (5) and posterior tibiofibular ligament (6).

On the distal side of tibia and fibula two ligaments (5 and 6) restrain the widening of the ankle mortise. On the proximal side the fibula is connected to the tibia with a number of ligaments that allow almost no freedom of movement. Moreover the tibia and fibula are connected along their length by a very stiff ligamentous membrane. The fibre direction is diagonally downward from tibia to fibula as Figure 2.3a shows.

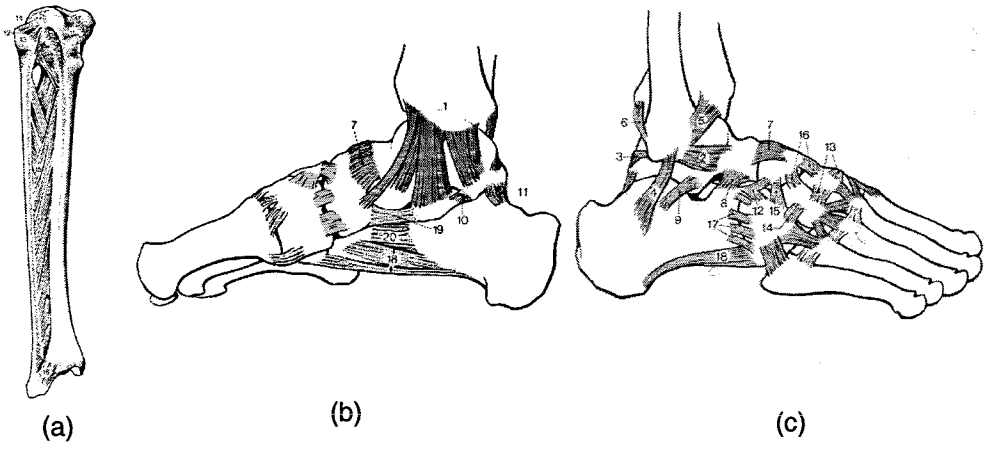

Figure 2.3: ligamentous structures of lower leg (a), ankle and foot from medial (b) and lateral (c) viewpoints

A connection from hindfoot to forefoot is made by the wide talonavicular ligament (7) on the dorsal side of the foot and by a number of long ligaments on the plantar side of the foot. The plantar foot ligaments restrain the expanding motion of the heel and ball of the foot that results from the distribution of the axial force from the leg to the two main points of pressure on the foot. These ligaments are: calcaneonavicular (19), calcaneocuboidum and longplantar ligament (18), the latter

in its turn can be subdivided in three branches extending to either tarsals or metatarsals. One tendon, called aponeurosis plantaris, also contributes to the restraint of the vault of the foot. It is connected to the distal tips of the metatarsals and to the bottom of the calcaneus. This tendon acts as a counterbalance for the plantar muscles in the foot that are responsible for the cringing of the foot.

Possibly the most important tendon in the lower leg is the calcaneus tendon, also referred to as Achilles tendon. A brief description of its function will be discussed in the paragraph below.

2.3 Muscles

The musculature of the lower limbs allows active movements through contraction and relaxation of muscle fibres. The muscles in the lower leg are responsible for the movements of the foot relative to the lower leg. The different movements of the foot can be subdivided in three rotational directions as indicated in Figure 2.4: dorsiflexion/plantarflexion, eversion/inversion and internal/external rotation. Muscles normally are responsible for a shortening movement in one direction as a result of active contraction. Simultaneously this muscle exhibits a passive resistance against elongation in the opposite direction.

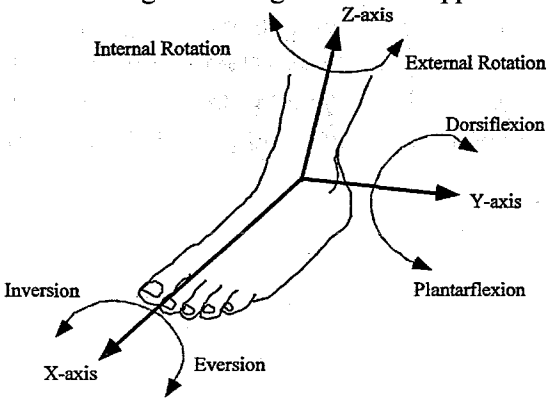

Figure 2.4: rotational directions of the ankle joint

The muscles of the lower leg can be subdivided in anterior and posterior position relative to tibia and fibula. The anterior muscles consist of a peronaeus group, responsible for internal/external and inversion/eversion movement, and an extensor group, responsible for active dorsiflexion and passive resistance against plantarflexion. The posterior muscles are composed of a superficial layer and a deeper layer. The deeper located muscles are partially responsible for active plantarflexion and passive resistance against dorsiflexion. Also they are to some extent responsible for movements in other directions. The superficial muscles are to a greater extent responsible for active plantarflexion movements. They exert the forces that allow people to stand, even on their toes. The muscles of the latter group are the medial and lateral gastrocnemius muscle and the soleus muscle (see Figure 2.5). On the proximal end the gastrocnemius muscles are attached to the distal femur on medial and lateral sides respectively. The soleus muscle is attached to a plate of tendon that attaches to tibia and fibula.

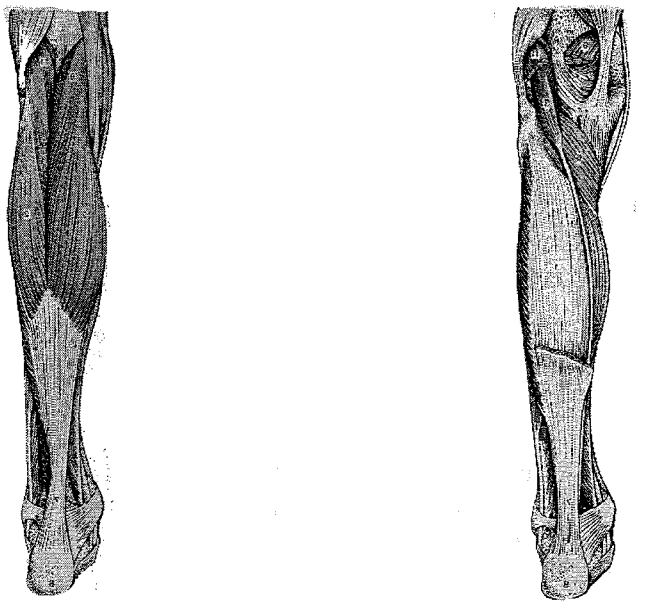

(a) (b)

Figure 2.5: superficial posterior musculature of the lower leg, gastrocnemius (a) and soleus (b)

The former named three muscles are on their distal ends connected to the calcaneus tendon, also referred to as Achilles tendon. This long and wide tendon extents from the calf to the hindfoot, where it attaches to the calcaneus bone. The dimensions of this tendon are dictated by the huge forces, up to 2 kN, that it transmits from muscles to skeletal system.

2.4 Plantar Tissue

The tissue on the sole of the foot is merely a build-up of layers of different tissue types. The bones of the foot are encapsulated by ligaments, while muscles are present for movements. The outer layer consists of fat and skin. Although plantar tissue is composed of these basic substances, special characteristics are often attributed to it [Bojsen-Møller, 1976] and [Sarrafian, 1983]. It functions as an interface between the stiff skeleton and the surrounding of the foot, often a shoe or floor. Under static conditions, like standing, it distributes the pressures from both irregular surfaces externally and bones internally. Under dynamic loading conditions, like gait and impact, it supposedly functions as a shock absorber.

3 Injuries, Injury Mechanisms and Tolerances

The lower leg is subject to injuries under many different circumstances. Collisions between pedestrians and vehicles often result in lower limb injuries, due to impact of the car's front with the legs. Vehicle occupants undergo high decelerations resulting in impact with interior parts in all types of crashes. This thesis is restricted to car occupant's injuries due to frontal impact only, since pedestrian lower limb injuries are the result of totally different injury mechanisms.

3.1 Injury Statistics

Over the last decade, the relative importance of car occupant lower limb injuries has increased. The introduction of restraint systems like belts and airbags resulted in a decline of head, neck and torso injuries, as Figure 3.1 shows. This figure consists of data from the US National Accident Sampling System (NASS). Morgan [Morgan, 1991] investigated 480 in-depth cases for the years 1979 through 1987. All cases were frontal impact crashes with either passenger cars, light trucks or vans. No rollover of the vehicle or ejection of the occupant occurred. All injured persons were over 16 years old and were front seat occupants. Both belted and unbelted situations were investigated. Pilkey [Pilkey, 1994] examined the NASS database for the years 1990 through 1992. From the year 1992 also cases with airbags became available. In both investigations only the six most severe injuries per injured person were considered, considering an injury severity of AIS 2+.

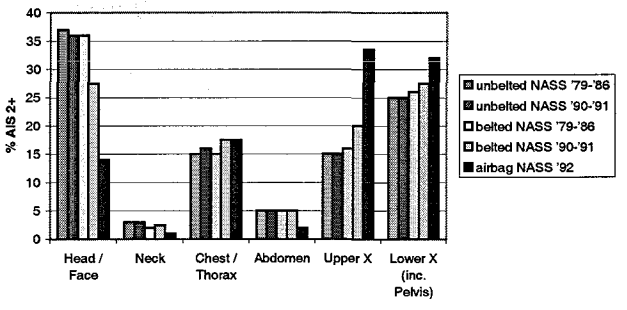

Figure 3.1: distribution of injuries with injury severity AIS 2+ by body region

In unbelted cases over 35% of all injuries were inflicted to head and face and just 25% to lower extremities. In belted cases a slight shift of importance towards both extremities occurs. The introduction of airbag restraint systems reduced head, face, neck and abdomen injuries seriously. The percentage of injuries to lower extremities increased to 32%.

Figure 3.2 shows the distribution of AIS 2+ injuries by region of the lower extremities, including the pelvis. The introduction of restraint systems resulted in a shift of distribution towards the lower leg, ankle and foot, whereas in unrestrained cases pelvis, thigh and knee injuries comprised the majority of injuries. For airbag

systems the percentage of injuries to lower leg, foot and ankle increases to 65% of all lower extremity injuries.

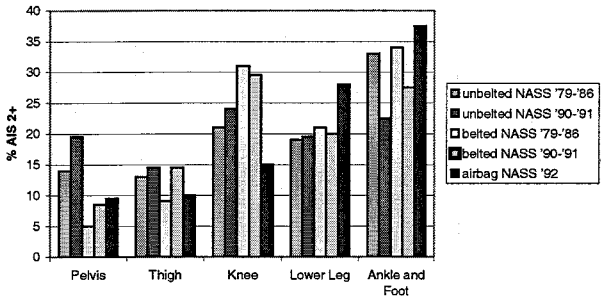

Figure 3.2: distribution of injuries to lower extremities with injury severity AIS 2+

Deducing from the importance of below knee injuries in frontal crash situations a further subdivision of body parts is denoted in Figure 3.3. For comparison also data from the Co-operative Crash Injury Study (CCIS), an in-depth database of accidents in the British Midlands, are included in this figure as derived from ADRIA [ADRIA, 1998]. A number of 112 below knee injuries inflicted to 65 drivers and 13 front seat passenger fulfil the following criteria: belted occupant, frontal impact, no rollover and AIS≥2.

A large percentage of injuries in the database are unspecified. Most AIS 2+ injuries are found in hard tissue expressed as fractures. It must be noted here that contusions and sprains are classified as AIS 1 and are therefore not visible in the figure below. It is evident that most fractures are present in the main line of force, running from the heel up to the knee. The calcaneus, talus, malleolus, distal tibia and fibula account for most of the specified injuries. It should be noted here that the metatarsals have a remarkable high share in all AIS 2+ injuries. An explanation for this occurrence can be found in Appendix A.

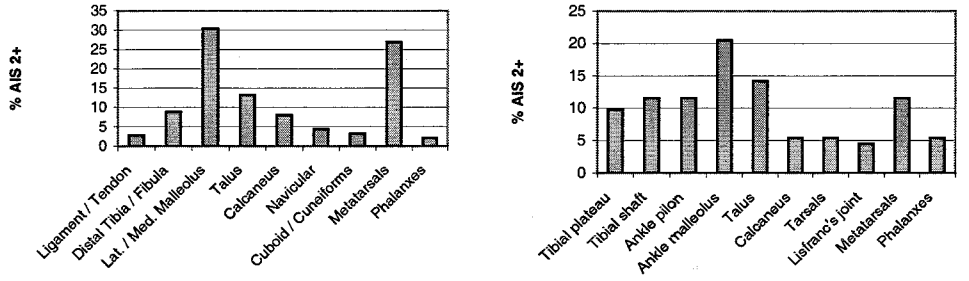

Figure 3.3: distribution of below knee injuries with injury severity AIS 2+ according to NASS data files (l) and CCIS data files (r)

Injury statistics is very much dependent on the boundary conditions of the accidents. Many different parameters have an influence on the probability of injuries. In literature the influence of intrusion, delta V and age are considered important. Therefore an overview of injury statistics concerning these parameters is given in Appendix A.

3.2 Injury Mechanisms

Injuries in frontal car crashes can have many different causes. The mechanisms through which injuries occur can be very widespread. This is due to the type and severity of frontal impact, the geometry of the leg compartment and the size and position of both legs in it. Morgan [Morgan, 1991] classified a number of accidents from the formerly stated NASS database into six mechanisms:

1. leg trapped between floor and instrument panel
2. foot contact with foot controls
3. wheel well intrusion
4. foot contact with floor
5. collapse of leg compartment
6. foot trapped under pedals

The figures below indicate that the majority of injuries are caused by a contact of the foot with the controls (mechanism 2). The second most probable cause is mechanism 4, a contact between foot and floor. Both mechanisms are caused by an acceleration of the occupant relative to the vehicle. It should be stated here that deformation of the interior compartment occurs only in mechanisms 3 and 5. It is also shown that intrusion is responsible for only 8% of ankle injuries and 13% of all foot injuries. In contrast to this, a sample from the CCIS database indicates that around 50% of all ankle/foot injuries are a consequence of intrusion.

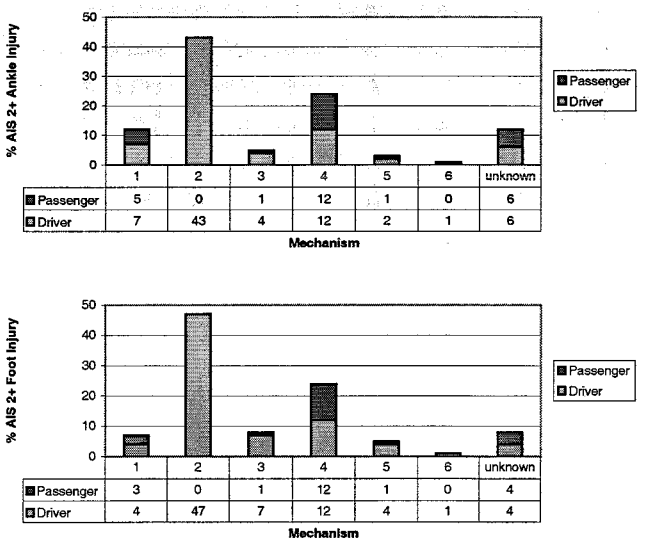

Figure 3.4: injury mechanisms associated with driver and occupant for ankle and foot injuries, according to Morgan [Morgan, 1991]

From Figure 3.4 it can not be concluded that more drivers sustain foot/ankle injuries than passengers do, caused by a limited sample size. Although not shown here, Morgan concluded that both drivers and passengers sustain more injuries to the right ankle (61% and 53% resp.) than to the left ankle (32% and 39% resp.).

In the former sections the types of mechanism that induced injuries were discussed from a vehicle point of view. The mechanisms in the human body that lead to

injury are reported by various authors. A number of loading conditions can be identified:

- vertical load: the load is applied to the heel of the foot, or to the whole foot. No ankle rotation is induced at first.
- dorsiflexion: an upward flexion of the foot. It is often induced by an impact to the forefoot
- inversion/eversion: an inward/outward rotation of the foot around its axis of length. It is mostly induced by impacting surfaces that contact the foot only on either side, or by impacting surfaces that are positioned under an angle.

From a number of 25 cases Lestina [Lestina, 1992] states that 15 injuries are due to inversion/eversion, 6 to direct vertical load, 1 to dorsiflexion and 1 due to a lateral-medial force. Half of the inversion/eversion injuries were caused by a contact of the foot with the pedals. These numbers are only indicative, since the sample size is too small to draw conclusions.

Morris [Morris, 1999] investigated the mechanisms behind different ankle and hind foot injuries. From 63 cases, he judged 23 cases to be caused by inversion/eversion, 13 by dorsiflexion, a remarkable 5 by plantarflexion, 18 by an axial load, 4 by avulsion and 4 by external rotation of the foot. In 4 cases a combination of dorsiflexion and inversion led to injury. Also he located the types of injury. Ankle malleolus fractures were caused by either inversion/eversion or external rotation. All ankle pilon fractures were due to an axial load, talus fractures were due to dorsiflexion or avulsion and calcaneus fractures were a result of axial load or avulsion. A fracture of the Lisfranc's joint in the foot was always caused by plantarflexion, a mechanism not often encountered in literature.

Otte [Otte, 1992] reported from a number of 108 cases almost 50% of the injuries to be caused to phalanxes and metatarsals. With a reference to Figure A.1b this indicates that this investigation included many cases were high intrusion levels acted, thus making it not a representative sample. Nevertheless conclusions can be drawn on the underlying injury mechanisms. All ankle joint fractures involved a rotation of the foot, calcaneus and talus fractures were caused by an axial load, whereas foot fractures were induced by both rotation and axial loading.

3.2.1 Influence of Inertial Loading

From an impact experiment to fifty amputated lower limbs, Crandall [Crandall, 1997] perceived a large number of malleolar and talus fractures occurred with the absence of large ankle rotations. This might suggest that the foot and ankle injuries described above can occur due to a combination of axial loading and a high rate of ankle rotation, while it may not require large ankle rotations by itself.

Lawson [Lawson, 1998] touches upon the influence of inertia for tibia fracture cases. A rapid acceleration of the foot on impact produces a high inertial axial force in the tibia, frequently followed by high angular acceleration about the knee. The latter produces high bending moments in the tibia.

3.2.2 Concluding Remarks

From the former general survey of literature three injury mechanisms are judged to be of primary importance:

- Axial loading of foot or knee in the direction of the tibia often leads to a crushed calcaneus, a fracture of the ankle pilon or fracture of the tibia due to bending.
- Dorsiflexion occurs from a load applied to the ball of the foot. The inflicted injury mechanism is crushing of talus or navicular bone.
- Inversion and eversion movements of the foot lead to malleolus fractures. Both ankle rotations are mostly due to tangentially oriented impacting surfaces or foot pedal contact. Also the natural tendency to eversion upon axial loading of the foot often results in malleolus fractures.

3.3 Injury Tolerances

Investigation on injury tolerances of the human lower leg has not been too extensive yet. Injury tolerances in the ankle and foot are difficult to measure due to the complex bone structure. Nevertheless Begeman [Begeman, 1990] reports a maximum dorsiflexion angle of 45°. Later it is proven from 10 cadaveric toe impact tests by Portier [Portier, 1997] that this value holds only for static loading. For this reason he reports an angle of approximately 30° in dynamic loading cases. The average measured ankle moment at which injury occurs is 60 Nm. Also investigations on inversion and eversion tolerances were executed. Begeman [Begeman, 1993] reported a failure angle of 60° with a standard deviation ±6° under dynamic loading. Parenteau's [Parenteau, 1998] more extensive work reported the following threshold values: 34.3° ± 7.5 and 34.1 Nm ± 14.5 for inversion and 32.4° ± 7.3 and 48.1 Nm ± 12.2 for eversion.

More research has been executed on tibia axial load. All tests are executed on human cadavers, where the differences with alive humans should be considered. Since it is generally agreed that muscle tension plays an important role under impact conditions the following numbers should be handled with caution. Kitagawa [Kitagawa, 1998] investigated the influence of Achilles preload on tibia injury tolerance. The axial force in the tibia was approximately the sum of Achilles preload and impactor force. From 16 cadaveric tests he determined the average impactor force to be 5132 N and the average measured tibia load 7645 N at which fracture occurred. The difference is therefore fully due to Achilles preload, although Kitagawa states an average value of 1500 N for this. Different authors approximate the value for maximum tibia load as stated above. Yoganandan [Yoganandan, 1996] reports 7830 N average, depending on age (see Figure A.3), and Begeman [Begeman, 1997] reports 7848 N on average.

Further investigation of Kitagawa on fractures in cadavers resulted in an average tibia axial force of 8115 N for calcaneus fracture and 7293 N for ankle pilon fracture.

4 Material Characterisation

One of the most important issues in human body modelling is material characterisation. The transformation of mechanical behaviour of tissue to a mathematical material law entails a severe simplification. Biological tissues are dependent on many factors, which cannot all be accounted for. In the following the translation of each type of tissue to an acceptable material law will be evaluated.

4.1 Bone

Bone as a tissue has extensively been investigated for its material properties by many researchers. The general opinion is that bone can be considered as linear elastoplastic material for small strains and that its behaviour is dependent on strain rate, density and age. In general a subdivision is made between cortical and trabecular bone, as stated in paragraph 2.1.1. The material properties of both tissues differ enormously. Therefore they will be discussed separately in the following paragraphs.

4.1.1 Cortical Bone

Cortical bone is found on the outer layer of all bones. In long bones it is typically orthotropic, thus different behaviour in longitudinal, radial and circumferential directions can be observed. For short bones orthotropy or anisotropy is of a minor degree. For all bones differences are observed under varying loading conditions, like tension, compression, bending, torsion and shear.

Elastic Modulus

Cortical bone is generally accepted to constitute linear elastic material behaviour for small strains [Yang, 1998]. From many investigations under many different test conditions it can be concluded that the mean elastic modulus of cortical long bones is 20 GPa with a standard deviation of 5 GPa. Table B.1 in Appendix B shows that bone is slightly stiffer under compression than under tension. Also can it be shown that tibia and fibula are in general stiffer than the femur. The values adopted for the model are shown in Table 4.1.

Plasticity and Failure

Plasticity is characterised by a yielding point. Material tends to yield at a certain amount of stress and strain. The work of Burstein [Burstein, 1976] is most extensive on this subject. He reports from 104-120 MPa for the femur and between 120 and 140 MPa for the tibia, as Table B.4 shows.

After yielding, fracture occurs at the ultimate stress of a material. Values for ultimate stress, as found in literature, are reported in Table B.2. The general view on long bone ultimate stress for different investigators under different loading conditions shows an average of 158 MPa with a standard deviation of 25 MPa.

4.1.2 Trabecular bone

Trabecular bone is characterised by its dependency on physiological and architectural conditions. Its sparse distribution through the matrix causes trabecular bone stiffness to be dependent on density and mineral content. Since only a mean value for trabecular bone material properties needs to be obtained for this model, no relationships for these factors need investigation. The assumption of trabecular bone being linear elastoplastic is sufficient for this thesis, since the influence of trabecular bone material properties will be proven to be negligible. Values as reported in literature for compressive properties of trabecular bone in tibia and femur are denoted in Table B.3.

4.1.3 Model parameters

The following table indicates the parameters adopted for the model. Values for femur, tibia and fibula stem from a validated three-point bending test on the same finite element mesh [Meijer, 2001]. Values for talus and calcaneus are average values found in literature.

Bone part	E (GPa)	σ_y (MPa)
Femur	**16** Cortical **0.013** Trabecular	**120** Cortical **35** Trabecular
Tibia	**43.8** Cortical **0.013** Trabecular	**196.5** Cortical **30** Trabecular
Fibula	**43.8** Cortical	**196.5** Cortical
Talus	**25** Cortical	**120** Cortical
Calcaneus	**25** Cortical	**120** Cortical

Table 4.1: material properties of different bone parts as adopted for the model

4.2 Ligaments and Tendons

Ligaments and tendons are strongly unidirectional soft tissues that have a high stiffness in one tensile direction and can withstand almost no forces in all other directions. This implies that a one dimensional representation is sufficient for these tissues. Prior research determined values for ultimate force, ultimate strain and linear stiffness, as denoted in Table B.5.

Although the table indicates linear stiffness values, it is agreed that ligaments constitute non-linear rate-dependent material behaviour. Attarian [Attarian, 1985] observed different failure limits for loading velocities varying from 0.00015

mm/ms to 1 mm/ms. Begeman [Begeman, 1996] tested the calcaneofibular and tibiotalar ligaments at cyclic loads up to 4 mm/ms and observed strain rate dependence, nonlinearity and hysteresis.

The development of mathematical models of rate-dependent materials led to linear spring dashpot configurations like Maxwell and Kelvin elements. Fung's quasi-linear viscoelastic (QLV) theory allows for a non-linear elastic response function [Fung, 1981]. Funk [Funk, 1998] determined material parameters for this QLV theory from experimental data on the eight most important ankle ligaments, as discussed in paragraph 2.2. The experimental data was obtained from 29 bone-ligament-bone specimens, dissected from fresh-frozen, near 50th percentile PMHS specimens, 45, 47 and 58 years old. The mechanical behaviour of the ligament model needs adaptation to high impact levels, occurring only at very high strain rates. For this reason a non-linear elastic curve was fitted to the QLV curve for strain rates of 1 mm/ms. The results of this fit are plotted in Figure 4.1.

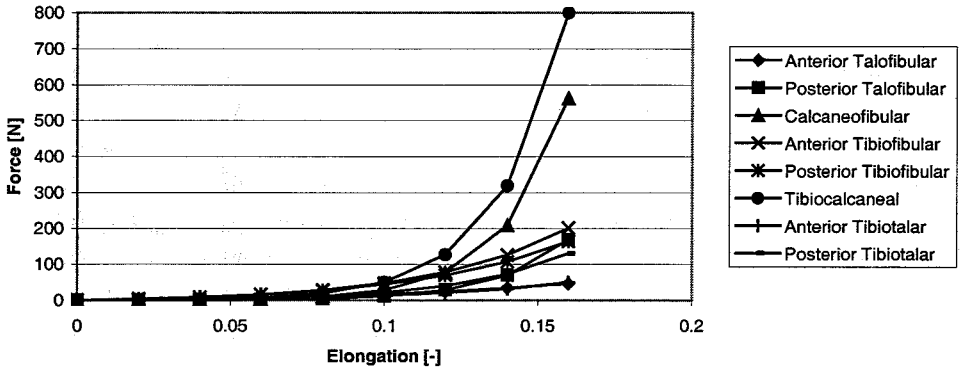

Figure 4.1: ankle ligament non-linear elastic curves

The Achilles tendon is known to be a stiff and strong tendon. Under impact conditions it rarely fails. This is due to its high stiffness, linear 982 N/mm [Hall, 1998], and high tensile strength, 1600-2000 N [Yamada, 1970]. This high stiffness causes Achilles tendon strain to be small, thus allowing a linear elastic material model.

4.3 Muscles

The mechanical behaviour of muscles is often represented in a Hill type muscle model [Hill, 1938]. The stiffness of a muscle is defined by a contractile element and a passive element. The contractile element is activated by the nerve system and the resulting force is dependent on muscle length and shortening velocity. The passive stiffness is a function of muscle length exclusively. Muscles always constitute their passive stiffness, while the active stiffness is due to awareness of car occupants, resulting in bracing.

The passive stiffness of the muscle group in the posterior leg, soleus and gastrocnemius, is determined by Hall [Hall, 1998]. After preconditioning the muscles were loaded with a peak load of 800 N at a quasistatic rate of 0.75 mm/s. After scaling with a 50th percentile man a second order regression curve was defined for both soleus and gastrocnemius:

$$F_{soleus} = 0.678x^2 + 1.022x \tag{4.1}$$

$$F_{gastrocnemius} = 0.570x^2 + 2.090x \tag{4.2}$$

Here the force F is defined in Newton and the displacement x is in millimetres. The standard errors were 0.8% for soleus and 9% for gastrocnemius.

The material properties applied in the model follow the non-linear elastic characteristic that Hall defined in the above equations. Since in the current model the gastrocnemius muscle consists of a lateral and a medial branch the force curve is distributed over the two branches in a 6:10 ratio [Cappon, 1999]. The force-elongation curves for the distinct muscles are shown in Figure 4.2.

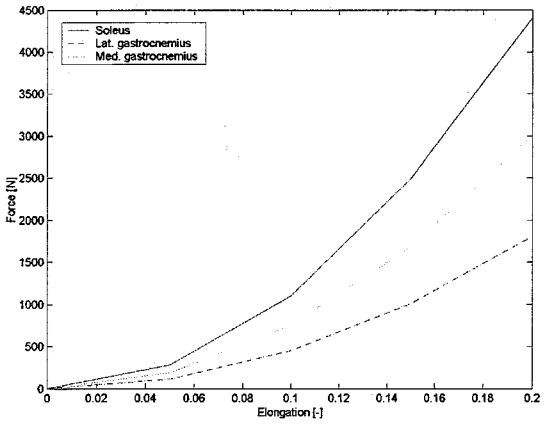

Figure 4.2: muscle non-linear elastic characteristics as derived from [Hall, 1998]

4.4 Plantar Tissue

A standard reference in plantar tissue experimental characterisation is Valiant's dissertation [Valiant, 1984]. He observed non-linear strain-rate dependent behaviour with serious hysteresis as Figure 4.3 shows. The size of the impactor is not specified, which removes the possibility to fit a curve on these experimental data.

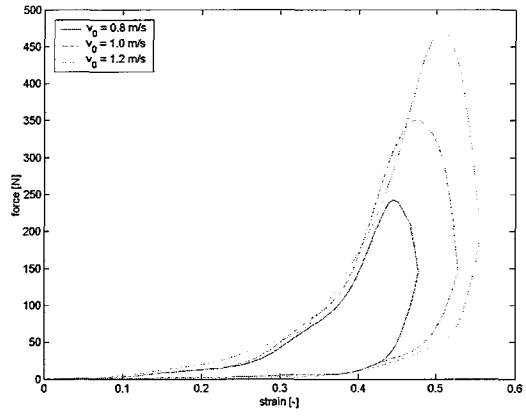

Figure 4.3: plantar tissue force-strain curves according to [Valiant, 1984]

Ledoux [Ledoux, 1999] developed a QLV relationship for plantar tissue and identified the parameters for seven areas on the sole of the foot from eight healthy cadaveric feet. He argued that all areas on the sole of the foot constitute approximately the same behaviour, except the subcalcaneal area. Peak forces rise up to 4 times higher there, damping constants are half that of other areas and the time constants are smaller too.

The implementation of strain rate dependant behaviour is left for further investigation. In this thesis a linear elastic model with hysteresis will be used, conform the following parameters:

- loading stiffness = 0.9 MPa
- unloading stiffness = 0.009 MPa
- hysteresis slope = 90 MPa

5 The Adult Lower Leg Model

In this chapter the adult lower limb model is discussed. This model exhibits the features of a human lower extremity from distal femur to toes. The model, which is implemented in MADYMO, consists of different types of structures, which are discussed separately in the following paragraphs.

5.1 Geometry

The geometry of the model is based on data obtained from the European HUMOS project [Serre, 2000]. Within this project a detailed coordinate description of all bone structures, flesh, skin, ligaments and muscles is collected in a mesh. The locations and dimensions of the structures are derived from a PMHS in driving position. The specimen was a 78 years old male. Its main characteristics are denoted in Table 5.1. For comparison the characteristics of a European 50th percentile male are presented in this table too.

	HUMOS PMHS	European 50th percentile male
Height (mm)	1730	1750
Sitting Height (mm)	920	915
Weight (kg)	80	75.5
Tibia Length (mm)	395.6	390.0

Table 5.1: main characteristics of different specimens, as taken from [Serre, 2000]

The lower limb model as discussed in this thesis ranges from distal femur to toes. Its structure is subdivided here in the following tissues: bone, flesh, ligaments and muscles. All are indicated in the figure on the following page.

5.2 Bone system

The composition of the bone system in the lower limb model is denoted in Table C.1 in Appendix C. The tibia and femur consist of different meshes. They comprise a distal and proximal epiphysis and a diaphysis. All bone parts exhibit compact bone behaviour, modelled as shell elements. Those elements lie on the outer surface of the bones. The epiphysis of femur and tibia also contain a spongy material description, modelled as solid elements and coloured dark pink in Figure 5.1. The outer layer of these solid elements shares its nodes with the shell elements. The importance of accounting for spongy material behaviour will be discussed in paragraph 7.1. The coarseness of the mesh can be deduced from the number of nodes and the number of elements as presented in Table C.1.

The bone mesh itself is further subdivided into different segments. The segments that describe the long bones and ankle consist of single bones according to their anatomical description, whereas the segments that describe the foot are a

combination of the bones in the anatomical regions: tarsals, metatarsals and phalanxes.

The subdivision into segments is of importance for modelling purposes. In the current model the long bone and ankle segments are implemented in a finite element description, whereas the foot segments are implemented in a multibody description. Both will be further outlined in paragraphs 5.2.2 and 5.2.3.

The positioning of the bone mesh, from its original seating position to a simplified standing position is executed by defining an imaginary joint axis in the ankle, according to Inman [Inman, 1976], and one in the knee.

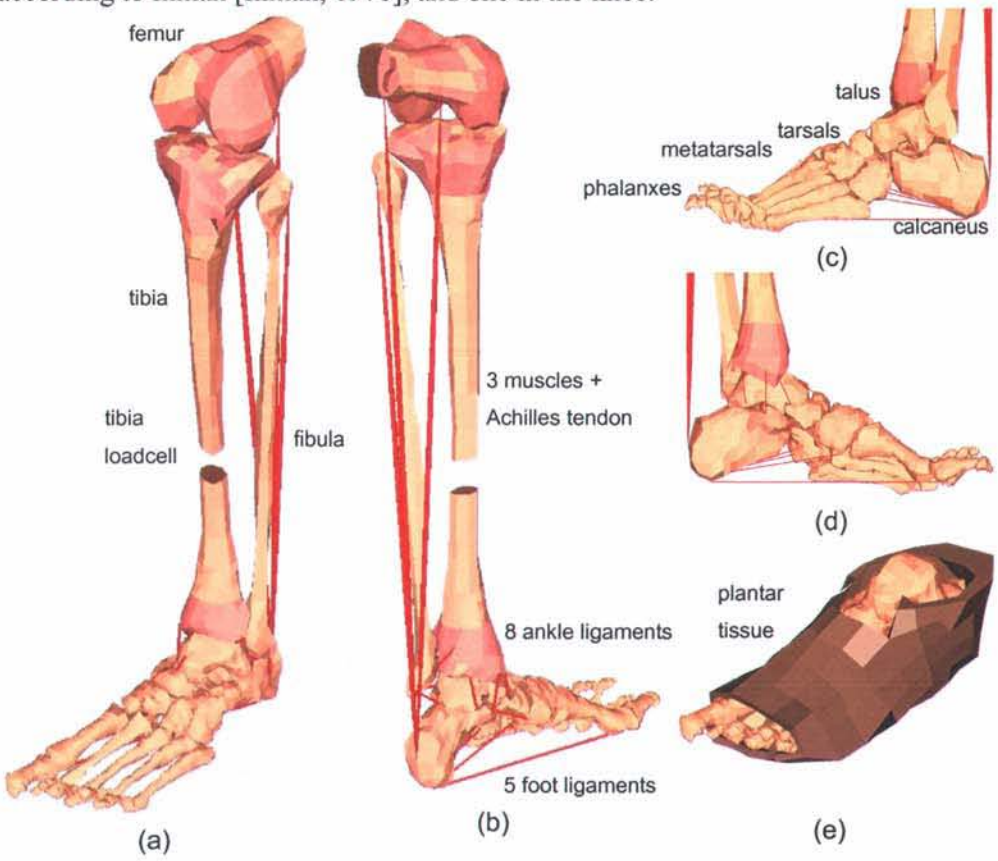

Figure 5.1: different views of the lower leg model; isometric view from front (a), isometric view from hind (b), from lateral (c), from medial (d) and with plantar tissue mesh (e).

5.2.1 Inertial Properties

Mass properties of the bone segments mentioned in Table C.1 are derived from [Hall, 1998]. Four 50^{th} percentile male specimens are examined for their mass properties with computed tomography scans. Boldface numbers in Table C.3 denote values obtained from [Hall, 1998]. Distal femur mass properties have not been adopted from literature, numbers are mere estimates. Tibia mass properties include soft tissues of the corresponding segment. In the current model no soft tissue is modelled for the leg segments in terms of mass and inertia. To account for mass properties of soft tissues, they are lumped in the tibia bone mass. Fibula mass

properties denote bone solely. The mass of the foot comprises both bone and soft tissue. Since soft tissue of the foot is explicitly modelled in the current model, the mass properties of both types of tissue should be subtracted. Lack of biomechanical data of the foot results in rough estimates of weight percentage bone constituent. The percentages and corresponding absolute values for mass of bone and soft tissues are denoted in Table C.3.

Inertial properties of the bone mesh are derived from HUMOS mesh properties. A MADYMO subroutine calculates the moments of inertia, centre of gravity and mass for a given mesh, element geometry and density.

Notion should be taken of the simplifications already made for modelling purposes. The lumped mass of soft tissue in the tibia bone mesh and the description of certain bone parts in thin shell elements instead of solid elements introduces more approximations. For a given shell element geometry, two design parameters are available for obtaining the needed mass: element thickness and density. Both parameters affect additional properties. A variation in element thickness influences the stiffness of the material and the moment of inertia, while a variation of density influences only the moment of inertia.

In the current model material properties are copied from [Meijer, 2001]. In the latter investigation the same mesh is validated against a three point bending test designed for pedestrian lower extremity impact simulation. Hence the combination of mesh, element thickness, elastic modulus, Poisson's ratio and yield stress are assumed to be valid for the current model. The remaining design parameter for obtaining the correct mass is density. Chosen values are denoted in Table C.4.

The bone segments of the forefoot - tarsals, metatarsals and phalanxes – are excluded from Table C.4 for they are not implemented as finite elements. Their inertial properties are described in terms of centre of gravity, moment of inertia and segment mass, rather than element thickness and density. Nevertheless a MADYMO subroutine calculated the required values, but they are implicitly used as model input for a multibody description.

5.2.2 Finite Element Modelling

The bone segments of the long bones and hind foot are implemented as finite elements, as mentioned before. It is assumed that in the main line of force deformations and local behaviour are important, in addition to kinematic behaviour. For a better understanding of injury mechanisms and criteria knowledge of stress/strain behaviour in ankle complex and tibia is necessary.

Two main types of material can be distinguished in bones: compact bone and spongy bone, often referred to as cortical and trabecular bone respectively. The cortical bone composes the outer layer of a bone, its thickness lies in the order of one millimetre. A quadrilateral shell element description is used for this material type. The elements can carry in-plane loads as well as bending loads [TNO, 1999].

The mass of the element is lumped in the four nodes, while fictitious mass moments are used. In Table C.1 the number of nodes and elements in the entire mesh are denoted. A total number of 1381 nodes and 1364 elements are used for the shell element description.

The inner constituent of a bone is trabecular bone and it is located mainly in the epiphysis. Its solid state makes a solid element description necessary. The solid element implementation in MADYMO consists of an eight node brick element that can carry tensile, compressive and shear loads. The solid elements are implemented in the epiphysis of femur and tibia. They exhibit a thickness of approximately 5 millimetres, and are attached to the shell elements by means of node sharing. A total number of 495 elements and 861 nodes is used for the three epiphysis. The importance of the modelling of trabecular bone will be discussed later.

Computational timestep is determined by the so called Courant stability condition, which accounts for element size, density and stiffness. The calculated minimum time step is $5 \cdot 10^{-7}$ s, which is used for the whole FE model. Finite element calculations take up 96% of the total computational time, which approximates 4 hours of CPU time on a SGI Octane R12000 with 300 MHz processor and 512 Mb internal memory, for each 100 ms simulation time. The timestep for multibody calculations is held within range of the FE timestep, to prevent numerical instabilities in the interaction between FE module and the multibody module.

The different bone segments are not constrained by kinematic joints. They behave as free bodies constrained by contact algorithms and soft tissue models that will be discussed in paragraph 5.3 to 5.6.

5.2.3 Multibody Modelling

The forefoot is the only bone system that is modelled as a multibody system. The deformations in tarsals, metatarsals and phalanxes are assumed to be less important than those in hindfoot and long bones. Under axial impact conditions deformations occur mainly in the main line of force, e.g. hindfoot and tibia. Only if dorsiflexion of the foot is involved some of the tarsal bones might crush. The navicular bone is likely to crush against the talus. The current model will not be able to predict the crushing behaviour of the navicular.

The kinematic behaviour of the forefoot is of primary importance for the response to impact. The foot exhibits stiffness or resistance to deformation, which induces a moment around the ankle joint due to inertial effects. The multibody model consists of three bodies, describing the three forefoot bone segments, interconnected by kinematic joints. The bodies exhibit mass, centre of gravity and moments of inertia as denoted in Table C.2. The shape of the geometry is defined by the mesh in a facet surface description. The geometry is rigid, but a contact function allows penetration and generates a contact force, the latter will be discussed in the next paragraph.

The connectivity of the multibody forefoot to the finite element hindfoot is realised by a constraint of the tarsal body, consisting of a contact description, ligaments and flesh and skin from the foot. The kinematic connection from tarsals to metatarsal is accomplished by a joint with a rotational degree of from freedom parallel to the y-axis. A rotational stiffness is implemented according to a former model [Hall, 1998] as shown in Figure 5.2a. The toe joint connects metatarsal bones to phalanxes by a single degree of freedom rotational joint. Its rotational axis constitutes a 18° offset angle from the y-axis, rotated around the z-axis. Its stiffness is denoted in Figure 5.2b. Both joints are slightly damped, with a damping coefficient of 0.17 N s m^{-1}.

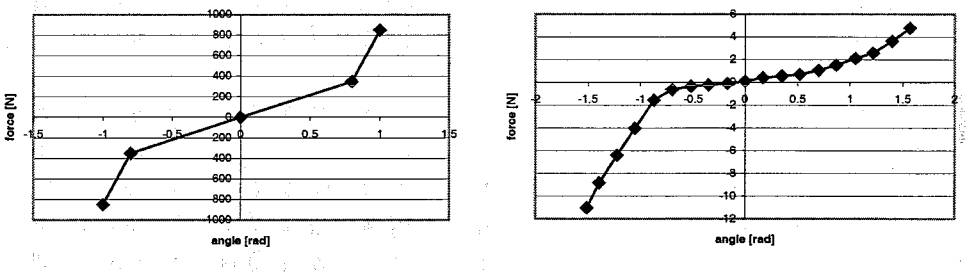

(a) (b)

Figure 5.2: joint stiffness of kinematic constraints in tarsal joint (a) and toe joint (b) according to [Hall, 1998]

5.3 Ligaments

The ligaments of the foot are all represented as multibody ligaments, meaning that a ligament is represented by a single spring element, which is connected to two nodes on each bone it connects. It constitutes the tension only non-linear elastic behaviour that is discussed in paragraph 4.2. Also hysteresis can be applied. The ligament can be initially pretensioned or slack can be defined. A drawback to this type of ligament is that connection to one node on each side might induce stress concentration in the finite elements around that node. All eight ankle ligaments are modelled according to this approach. The non-linear elastic curves from [Funk, 1998] are adapted and ligaments are pretensioned to 110% for model stability. No experimental proof is available on this number, but ligament pretension is observed in vivo.

Furthermore it should be noted here that the mechanical behaviour of the membranous ligament between tibia and fibula is lumped in a three-degree-of freedom spring damper element that connect proximal fibula and proximal tibia. The mechanical properties are derived from [Meijer, 2001], meaning 1553 N/mm loading stiffness in all directions, a hysteresis slope of 4.637 N/mm and an unloading stiffness of 155.3 N/mm. The applied damping constant is 2.0 N s m^{-1}.

5.4 Muscles

The three muscles discussed in paragraph 2.3 are modelled according to a subroutine in the MADYMO code. They constitute a Hill type muscle model, to which active characteristics can be applied. The non-linear elastic passive stiffness characteristic is described in paragraph 4.3. The muscles connect to one node on the posterior surface of the calcaneus on their distal end. On the proximal side the soleus is connected to the fibula, while anatomy prescribes a connection to a large plate of tendon that connects fibula, tibia and femur. The two branches of the gastrocnemius muscle are connected to two nodes on the medial and lateral sides of the distal femur. In the current model, muscles act as non-linear tension-only springs, a behaviour also observed in post-mortems and unaware volunteers. Active muscle behaviour occurs in real life accidents, as people tend to brace, and in tests with aware volunteer tests as will be discussed later.

5.5 Plantar Tissue

The plantar tissue is explicitly modelled as a finite element mesh, consisting of 361 nodes and 204 solid elements. This mesh, obtained from HUMOS, represents not only the plantar sole of the foot, but also the flesh in the whole foot, thus constraining movements of the foot skeleton.

The density of plantar tissue is derived from the density of fat tissue, 1630 kg m^{-3}. The solid elements calculation is fast due to its reduced integration method with one integration point, but it might induce hourglass modes.

Here a linear elastic stress-strain characteristic is used with hysteresis. The finite element code used here is developed for materials that undergo high compression, reducing the element thickness to approximately zero. This phenomenon is frequently observed in plantar impacts, as impacting surfaces nearly reach the relatively rigid calcaneus or metatarsal bones. The physical incompressibility is not accounted for, since the stress-strain characteristic is a one-dimensional quantity.

5.6 Contact Description

As mentioned before a contact description restrains the relative movement of different bodies in the model. Two types of contact can be distinguished in the model: bone-flesh contacts and bone-bone contacts.

Bone-Flesh Contact

Bone-flesh contacts are present in the entire lower leg. Since it is assumed that only the flesh at the sole of the foot affects the mechanical behaviour, only contacts with bones of the foot is defined. The bones of the forefoot are supported to the flesh, thus the remaining bones contacting flesh are talus and calcaneus. In order to provide a stable contact algorithm for all loading cases a penalty contact has been used. A contact force F_c is generated depending on a number of parameters. The

constitutive material law is implemented by taking the bulk modulus K of the soft tissue. The contact geometry is taken into account by using the initial volume V_0 and area A of the contact segment. A penalty factor ζ is defined in equation (5.1), which allows for tuning of numerical stability. Another tuning parameter C_{maxfrc} scales the element thickness t_e in order to compare it with the penetration depth λ. The minimum value from this comparison dictates the generated contact force. Thus a limited contact force is provided for in the algorithm, ensuring more stability in the calculation.

$$F_c = \frac{K}{V_0} A^2 \zeta \min\left(\lambda, C_{maxfrc} \cdot t_e\right) \tag{5.1}$$

For both contacts defined in the model default values for penalty factor (ζ=0.1) and maximum force limitor (C_{maxfrc}=1) are adopted.

Bone-Cartilage-Bone Contact

As described in paragraph 2.1.3 there are many bone to bone contacts present in the lower leg. All contact surfaces are covered with a layer of cartilage. The mesh, as described above, describes the bone geometry, so initially there is a gap between two bone surfaces in the mesh. This gap constitutes cartilage material behaviour by using an algorithm that generates a contact force before nodes enter the surface defined by the mesh. The code does not allow for a variable gap thickness for each contact segment. Therefore the mean distance between two mesh surfaces is estimated. This distance is shown in Table 5.2. The determination of the mean distance causes a number of nodes to lie initially within the gap, resulting in an initial contact force generated by the algorithm. A procedure is setup for driving those nodes out of the gap to avoid initial forces, thus obtaining an initially stable mesh.

Elementset	Nodeset	Gap thickness [mm]
Femur	Tibia	2.0
Femur	Fibula	0.0
Tibia	Fibula	3.3
Talus	Tibia	1.0
Talus	Fibula	1.0
Calcaneus	Fibula	0.0
Calcaneus	Talus	1.0
Talus	Forefoot	0.5
Calcaneus	Forefoot	0.5

Table 5.2: gap thickness for contacting surfaces in bone-cartilage-bone contact

The contact algorithm generates a contact force F_i per node i according to equation (5.2).

$$F_i = A_i\left[\sigma_e + f_d\left[C_d \frac{\lambda_i}{t_i} + \sigma_d\right]\right] \tag{5.2}$$

This force is dependent on the area A_i of the elements that are connected to the node i. Furthermore it is dependent on an elastic stress characteristic σ_e, which

depends on the ratio between penetration λ_i and thickness t_i of the elements connected to the node. The first part of the curve (Figure 5.3b) represents the soft cartilage. This curve is derived from quasi-static experiments by Hori and Mockros [Hori, 1976]. The second part of the curve (Figure 5.3a) represents the much stiffer bone. The contact stiffness might even approximate infinity, since finite element material deformation becomes responsible for further stress-strain behaviour.

The remaining parameters, with subscripted d's are damping terms. Since cartilage is a gel-like tissue it is much stiffer for higher loading rates. This allows for an application of a damping coefficient of 1000 N m^{-2} s^{-1}, which physically causes damping forces to be 10 times smaller than elastic forces at average impact speeds.

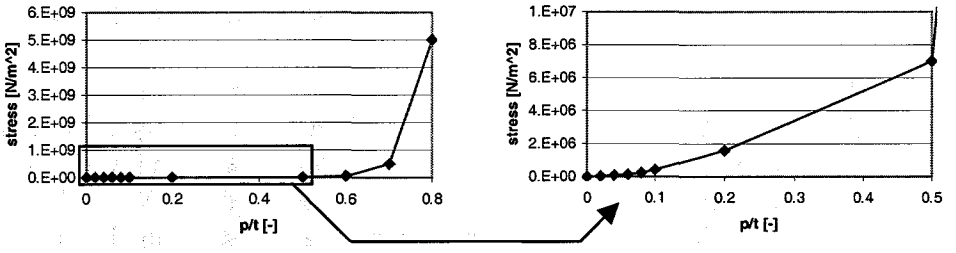

Figure 5.3: elastic stress as a function of the ratio between penetration and element thickness for bone-cartilage-bone contact

6 Evaluation of the Adult Lower Leg Model

In this chapter the results are presented of the evaluation of the global response of the lower leg model. The experimental test setups are described for two types of tests. The modelling of these test setups is described afterwards and finally the results are presented. For a discussion on the results presented here, it is referred to paragraph 9.1.

6.1 UVa Tests

The Automobile Safety Laboratory of the University of Virginia - Charlottesville, Virginia, USA – performs experiments for automobile safety purposes using both dummies and post mortem human subjects (PMHS). Some of the resulting data will be used for validation of the model under severe impact conditions.

6.1.1 Experimental UVa Test Setup

The UVa test setup, as depicted in Figure 6.1, consists of a stiff frame, a knee restraint system, a footplate system and a pendulum. The SAE sign convention is used for this apparatus, thus defining an x-axis pointing anteriorly along the line of the second metatarsal, an y-axis pointing to the right and a z-axis along the line of the tibia in distal direction.

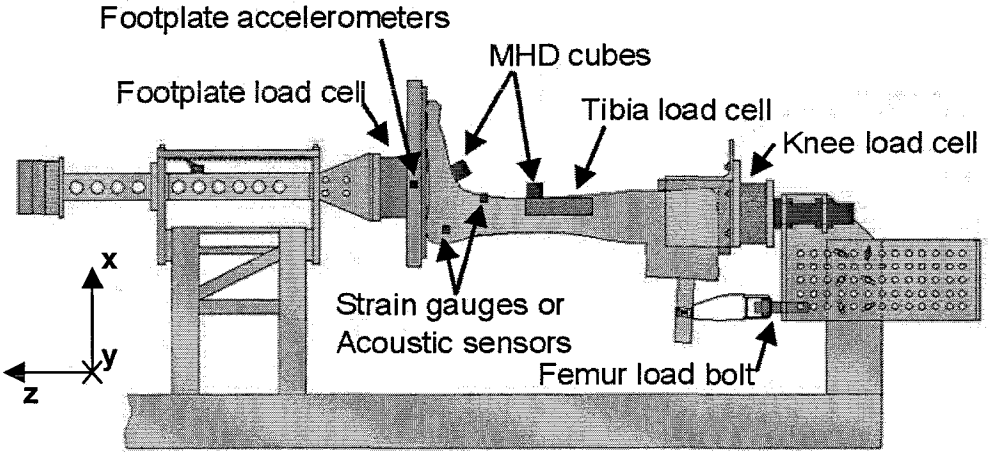

Figure 6.1: UVa test setup for cadaveric lower limbs

The knee restraint system consists of four plates, all padded with poly-urethane foam of 25.4 mm thickness, restraining movement of the knee in three translational directions. A 6-axis loadcell is applied in the kneeplate system, measuring forces and moments. The system is mounted to the frame with a pretensioning bolt, allowing clamping of the lower leg. Furthermore a load bolt is mounted to the knee restraint system and connects to the femur, just below the dissection. The linear spring restrains flexion movements of the knee joint. The force guided through the load bolt is also measured.

The footplate system consists of a single plate, padded with one or two layers of 9.5 mm foam. Between the footplate and the transfer piston a loadcell measures 3 forces and 2 moments. The transfer piston translates freely, as it is struck by a pendulum. An accelerometer, mounted on the footplate, measures the acceleration of the footplate in three directions, while an accelerometer in the transfer piston measures accelerations in z-direction only.

The lower leg is positioned in between knee- and footplate like in a straight seating posture, meaning that the angle between foot and lower leg and the angle between lower leg and upper leg both equal 90 degrees. The PMHS lower leg itself is mounted with a number of sensors. A loadcell is implanted in the tibia, replacing bone along approximately 9 centimetres of tibia length. Two cubes with tri-axial magneto-hydrodynamic (MHD) angular rate sensors and tri-axial accelerometers are applied for acceleration and ankle rotation measurements. One cube was mounted to the tibia load cell assembly, the other is screwed to the navicular, medial cuneiform and first metatarsal bones.

In order to test the influence of passive muscle behaviour a slightly modified test setup is designed, as Figure 6.2 shows. A cam cleat is used to grip the Achilles tendon. The cam cleat is attached to the frame by means of a rope via a pulley, a constant force energy absorber and a load cell. Initial pretension is applied to the Achilles tendon thus lifting the foot from the footplate. In order to compensate for this lifting the kneeplate preload is increased.

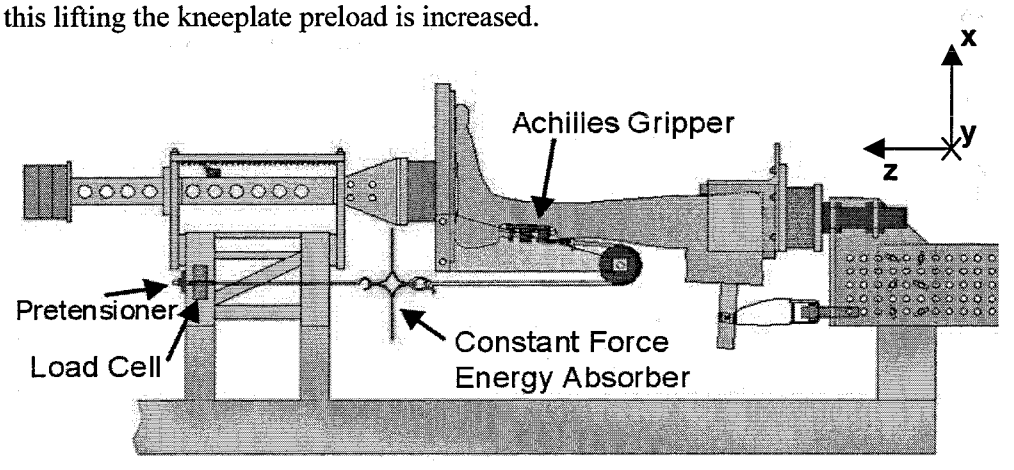

Figure 6.2: UVa test setup for cadaveric lower limbs with simulated muscle tension

6.1.2 Modelling Of UVa Test Setup

Implementation of the experimental test setup in the current model is achieved by applying boundary conditions prescribed by the experiments. The knee- and footplates are physically implemented as planes with a rigid FE mesh, called facets in MADYMO. This allows for a facet-node contact description. The mechanical properties are adopted from foam force-displacement experiments and expressed in stress versus relative penetration curves (see Figure 6.3). A constant friction coefficient μ of 0.7 is applied throughout. The linear displacement of knee- and footpad is enabled by introducing two translational joints.

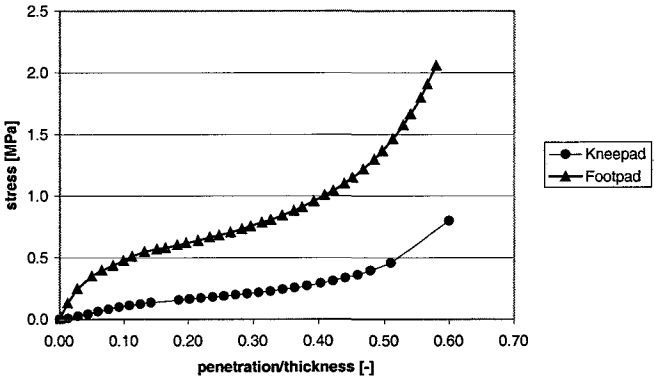

Figure 6.3: stress / relative penetration curves for foot- and kneepad from experiments [Funk, 2000]

The femur load bolt is modelled as a linear spring, attached to a number of nodes at the proximal end of the femur dissection. The stiffness, derived from experimental observations equals 850 N/m, whereas the force in the spring is measured as a function of time.

Load cells are incorporated in the model by means of bracket joints, where output is generated for all transmitted forces and moments. In the tibia the continuum is subdivided by deleting a number of elements (see Figure 6.4), thus obtaining two bone parts interconnected by a bracket joint.

The load cells in both foot- and kneeplate are situated in the pistons at locations comparable to those in the real test setup.

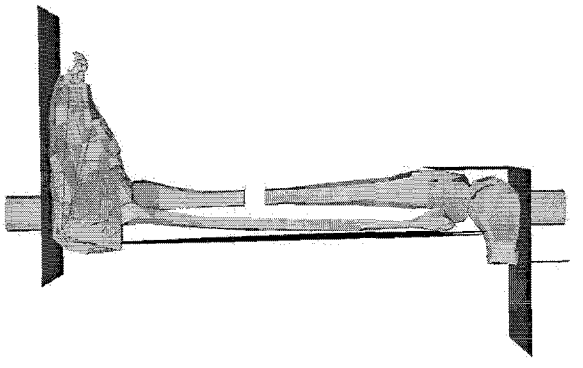

Figure 6.4: model of UVa test setup

The two accelerometers are implemented in the model for measurement of linear accelerations. The foot accelerometer is attached to the body describing the metatarsals. The tibia accelerometer is attached to the bracket joint describing the tibia loadcell. Both accelerometers are positioned at a similar locations in the experiments. Ankle rotation is determined from the relative positions of the two MHD cubes.

The initial clamping of the lower leg in the modelling environment is correctly applied by quasi-statically (within 300 ms) translating the kneeplate until force measurements in the footplate are equal to those of the experiments at time zero.

The experimental impactor pulse, induced by the pendulum to the footplate, is used as the input for the impact simulation. No physical pendulum is modelled, the acceleration pulse resulting from pendulum impact is used as an input signal for the translational joint in the footplate. The same modelling simplification is adopted in the muscle pretension test setup. The force measured in the load cell of the experimental test setup is used as an input signal for the Achilles tension. Thus the Achilles tension is applied to the muscles in the model. Here a difference in boundary conditions arises, since in the experiment muscle pretension is considered as an external force, whereas it acts internally in the model. Simulations proved that this difference does not alter the response of the model.

6.1.3 Results of UVa Tests

The model will be evaluated against 5 different UVa tests. In the following the tests are denoted with a characteristic number: 3a, 5c, 5d, 6i and 7d. Their most important characteristics are presented in Table D.1 in Appendix D. Measured responses from both experiment and model comprise the parameters presented in Table D.2. The signals of importance will be discussed here, for the rest of the signals it is referred to Appendix E.

Input signal

The acceleration of the footplate functions as the input signal for the simulation, together with the resulting displacement. Both signals are plotted in the following figure.

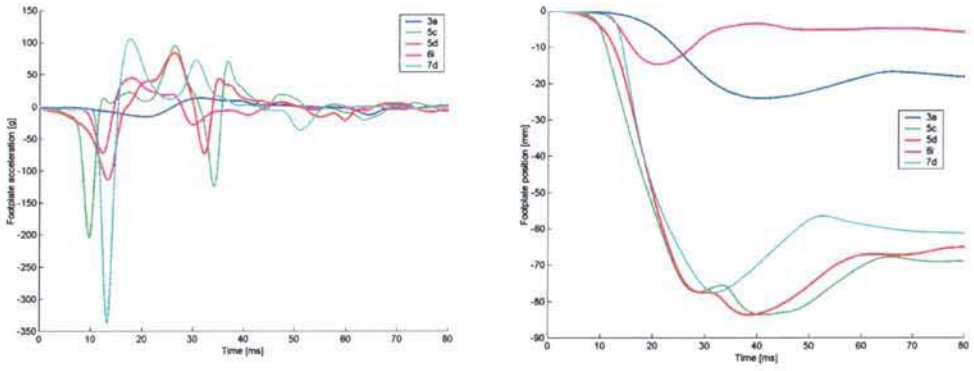

Figure 6.5: footplate acceleration (l) and displacement (r) for 5 UVa experiments, with their characteristic numbers denoted in the legend

For experiments 6i and 7d muscle pretension is applied, where the Achilles load functions as another input signal. It is therefore plotted in the following figure.

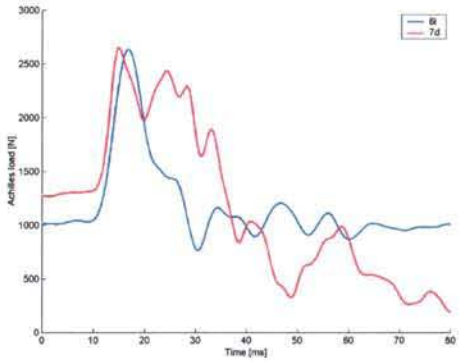

Figure 6.6: Achilles pretension input signal

External forces

The measured external loads consist of forces and moments measured in the foot- and kneeplate loadcells, femur load bolt and in the experimental cases also in the Achilles loadcell. Loadcell moments can not be compared since the exact location of the lower leg with respect to the loadcells is unknown. A valid comparison between loadcell forces is impossible for experiments 6i and 7d, caused by the difference in Achilles boundary condition modelling, as discussed in paragraph 6.1.2.

Tibia loadcell

The tibia loadcell response comprises three force measurements and two moments. Figure 6.7 shows plots for axial force F_z. Generally the peak force is well simulated, except for experiment 5c and 7d where failure occurred. Note the initial fluctuation in the loadcell of simulation 3a.

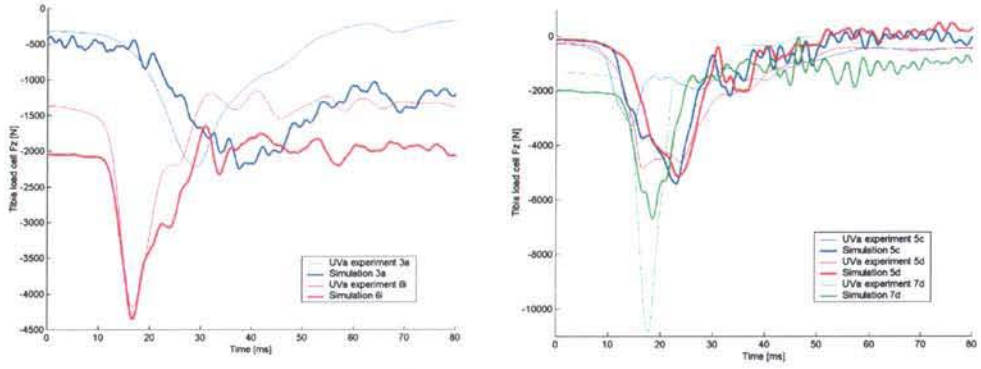

Figure 6.7: tibia loadcell axial force for medium severity experiments (3a,6i) and from high severity experiments (5c,5d,7d)

The other signals, F_x, F_y, M_x and M_y are shown in Appendix E, since they are of little value for this research, as will be discussed later.

Ankle rotations

Kinematic responses of the foot resulting from impacts are described by ankle rotations in three directions, resulting in dorsiflexion, eversion or internal rotations or their counterparts (see Figure 2.4).

The figure below shows dorsiflexion responses. For all simulations the dorsiflexion angle is significantly higher than it is for the experiments.

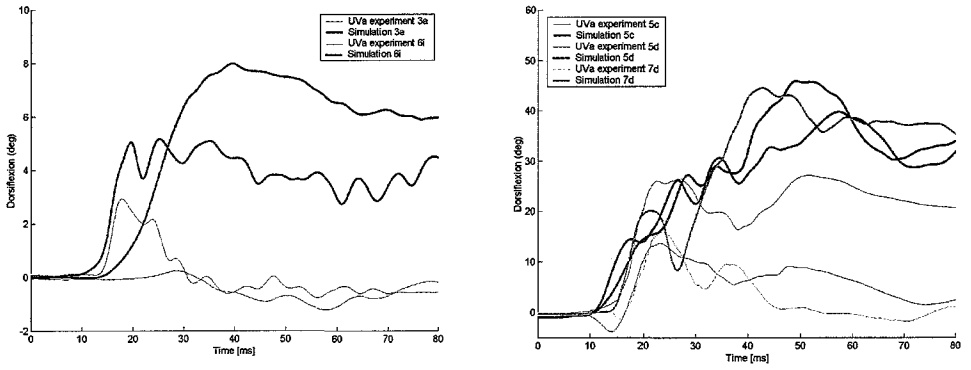

Figure 6.8: ankle dorsiflexion angle from medium severity experiments (3a,6i) and from high severity experiments (5c,5d,7d)

Figure 6.9 shows the eversion angle. Simulations follow the general trend of initial eversion upon axial impact, followed by inversion for high severity impacts.

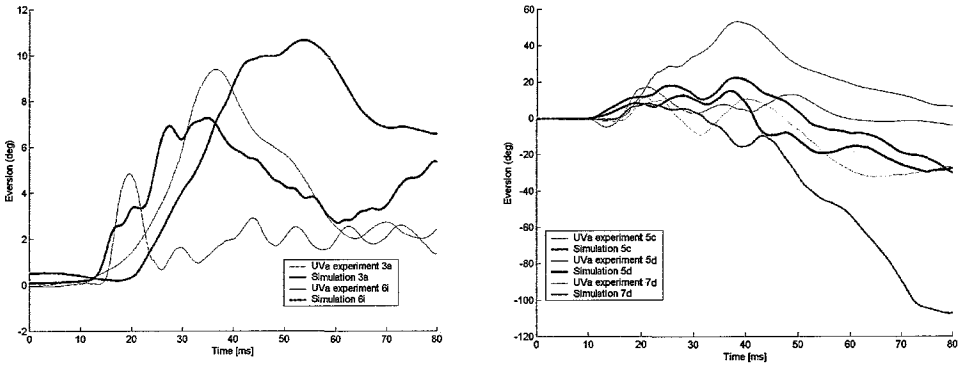

Figure 6.9: ankle eversion angle from medium severity experiments (3a,6i) and from high severity experiments (5c,5d,7d)

6.2 TRL Tests

A different evaluation approach stems from experiments performed at the Transport Research Laboratory (TRL) in the United Kingdom. Data is obtained from pendulum impact tests performed on both PMHS and volunteer lower legs. This data is used for evaluation of the model under low impact conditions.

6.2.1 Experimental TRL Test Setup

The test setup, developed by TRL, consists of a supporting structure for the leg and a pendulum rig, as Figure 6.10 depicts [Manning, 1998]. The lower leg is positioned horizontally with both knee and ankle joint 90° flexed. The foot rests on a rigid block covered with a PTFE polymer sheet. With the pendulum different locations on the sole of the foot can be impacted. The pendulum consists of an impactor and an arm. The impactor is a cylinder with a 25 mm radius and 1.25 kg mass, while the arm has a length of 1 m and weighs 285 g. The effective impact mass is 1.4 kg.

On this rig experiments are executed with PMHS and with unaware volunteers. The PMHS lower legs were initially fresh-frozen and then thawed for over 24 hours. A length of 12 cm of tibia bone was substituted with a Denton^{TM} tibia loadcell. A special insertion technique allowed for exact alignment whilst maintaining structural integrity [Manning, 1998]. Volunteer tests were executed with volunteers that were blindfolded and wore headphones with loud music. It is assumed that muscle reflex responses do not occur within 100 ms prior to impact, due to relatively long reflex pathways and an electromechanical delay [Siegmund, 2000]. The result is an unaware volunteer experiment where pre-impact bracing is of no influence.

The pendulum location was altered to impact the toe or heel or to impact the medial or lateral sides of the foot. For toe and heel tests the heel of the foot rested on the rigid block, whereas for lateral impact the foot rested on its medial side and for medial impact the foot rested on its lateral side. Tests have been executed at three different speeds of impact; 2 m/s, 4m/s and 6 m/s. It should be noted here that unaware volunteer tests consist of toe impact tests only at speeds of 2 and 4 m/s.

6.2.2 Modelling of TRL Test Setup

The test setup from TRL is modelled by resting the foot on a plate with a node-facet contact description assuming a Young's modulus for PTFE of 400 MPa. The input for the simulation is the speed of the impacting cylinder just before impact. The cylinder is also described by a facet geometry that is assumed rigid. The mass of the arm of the pendulum is lumped in the mass of the cylinder. The tibia loadcell used here is exactly the same as used in the model of the UVa test setup, thus not fully representing the TRL loadcell. Ankle rotation is measured as described in paragraph 6.1.2 and an output signal channel is reserved for pendulum acceleration.

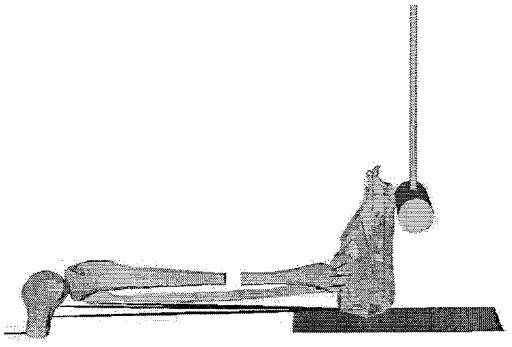

Figure 6.10: model of TRL test setup

6.2.3 Results of TRL Tests

Pendulum acceleration

The pendulum acceleration response to 4 m/s impact is depicted in Figure 6.11 for both PMHS and volunteer tests. The peak is well simulated, while a bouncing effect arises afterwards.

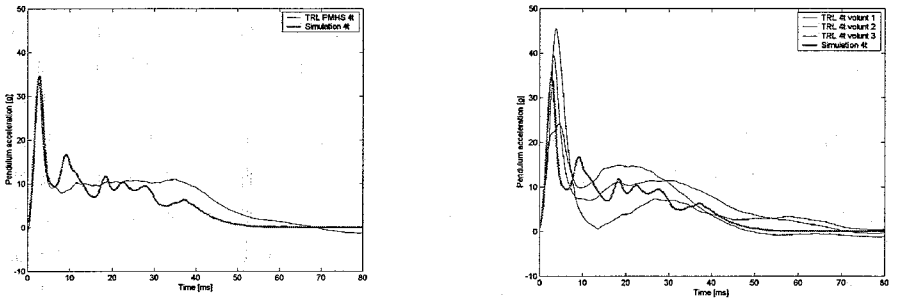

Figure 6.11: pendulum acceleration response for PMHS (l) and volunteer (r) tests

Dorsiflexion

The most important response from a toe impact test is of course the dorsiflexion angle. For an unknown reason no dorsiflexion angle is reported for PMHS tests. For three volunteer tests this angle is shown in the following figure.

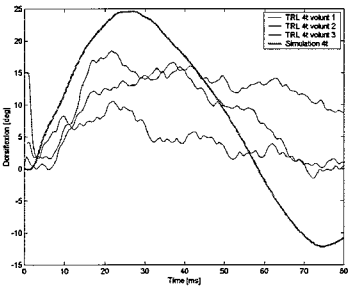

Figure 6.12: dorsiflexion response for volunteer tests

Tibia loadcell

For PMHS tibia loadcell responses it is referred to Appendix F, with an additional explanation on occurring vibrations in paragraph 7.5

7 Parameter Sensitivity Study

The model, as discussed in chapter 5, is realised by translating a large number of physical properties into mathematical descriptions. Not only is there a large spread in physical properties among the sample population, also the transformation into mathematical descriptions brings in a large parameter uncertainty. This chapter deals with the sensitivity of certain important parameters to changes in the response of the model, in order to justify the chosen parameters and to define biofidelity ranges.

7.1 Bone Properties

The properties of the bone mesh are subject to parameter variation since the shell element description incorporates large assumptions.

At first the influence of the solid mesh used for trabecular bone is discussed. Since its stiffness is 1000 times smaller, the influence on the total bone stiffness and global response is negligible. But since it functions as filling in the diaphysis, it influences the local stress distribution. If no solids are modelled, more deformation occurs in the diaphysis. In reality the trabecular bone is present in all bone parts, so it should have been modelled in all bone parts where compression plays a role.

The yield stress in the model is used as a parameter for injury assessment. The values are taken from literature references, but they vary in a wide range. Variation of this parameter will control the occurrence of injuries at specific locations, and is altered only for injury prediction purposes.

The Young's modulus determines the elasticity and resulting temporary energy storage of the bone mesh. A variation of the elastic modulus between 20 and 45 GPa does not significantly alter the global response or temporary energy storage, thus no influence is attributed to this parameter within its ranges.

7.2 Cartilage Contact

The used cartilage contact model is based on the contact algorithm implemented in the MADYMO code. The contact between two bone surfaces is defined by a stress-penetration characteristic derived from quasi-static experiments. Under impact conditions the compressive stiffness is reported higher [Oloyede, 1992]. Therefore a simulation is executed with tenfold increased cartilage stiffness. The global response to axial impact in terms of force does not differ much, since the cartilage behaviour is responsible for approximately 4 mm of the 80 mm total footplate displacement. Differences do occur in the kinematic ankle joint response. The stiffer contact model allows less freedom of movement of different bone parts with respect to each other. This results in 5° smaller dorsiflexion and eversion angles, which increases biofidelity.

7.3 Ligaments

In the model development stage an alternative to the multibody representation of ligaments was proposed. In this case ligaments are modelled using a finite element approach, as Figure 7.1 shows. In the mesh obtained from HUMOS [Serre, 2000] the eight most important ankle ligaments are modelled as quadrilateral membrane elements. The advantage of a finite element ligament is its wider attachment to the bone parts. An linear elastic isotropic material model is applied. The Young's modulus is determined from the force-elongation relationships from paragraph 4.2 and from the mean surface cross section and length of each ligament. The finite element ligaments are curved around the bone surfaces. Upon ligament loading the element stretches towards the bone mesh. Therefore a contact is defined between ligament and bone mesh. This ligament definition is rejected in the end because of the less accurate model description. At first the FE ligaments are linear elastic isotropic materials, whereas the multibody ligaments constitute tensile only non-linear elastic material behaviour with hysteresis and pretension. In addition the curved geometry of the FE ligaments disables pure tensile behaviour.

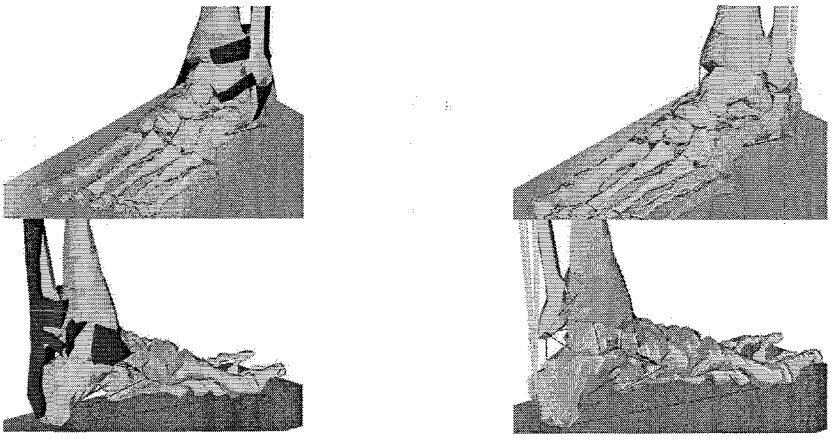

Figure 7.1: different ankle ligament approaches; finite element membrane elements (l) and multibody non-linear spring elements with hysteresis and pretension (r)

The chosen 10% pretension of the ankle ligaments is evaluated by comparison with a non-pretension simulation. The pretension causes the ankle joint to become stiffer, thus reducing ankle rotations with approximately 5°, causing increased biofidelity.

7.4 Plantar Tissue

In the current FE model a non-linear elastic characteristic with hysteresis is used for plantar tissue. The effects of hysteresis are judged from the pendulum acceleration curve of TRL experiments. If no hysteresis is applied the pendulum bounces against the plantar tissue, whereas the current hysteresis model causes a smaller bouncing effect, judging from Figure 6.11. Since the current hysteresis model approximates a zero unloading curve the bouncing effect can only be further reduced by application of damping in the current plantar tissue material model.

7.5 Vibrations

In many global response signals from all simulations a number of vibrations occur that do not correspond to experimental findings. In UVa tibia loadcell force and moment signals a resonance with a typical period time of 8 ms disrupts the global response. For TRL tests the general period time of resonances approximates 5 ms. The following parameter variations have been executed in order to reduce these vibrations, so far unsuccessful:

- A first approach in vibration reduction is adding damping. Damping can be applied to contact interactions, ligaments or to nodes of the bone mesh. Simple simulations proved that damping in contacts or ligaments can not fully compensate for the non-physical vibrations. This is due to the small excitations both multibody models make. It was also proven that no numerical instability occurred in the contact function, causing the vibrations. Nodal damping can reduce any vibration, but then any physical representation vanishes. In fact nodal damping adds inertia to the bone mesh for certain frequencies, thus slowing it down.

- Another cause for vibrations could be the free body geometry of the ankle joint. A number of single degree of freedom mass-damper-spring systems are constructed connecting different bone parts in order to determine a possible cause for the vibrations. The tibia was assumed to be rigidly supported. The bone contacting the tibia is the vibrating mass and the contact stiffness and ligaments are represented by a spring and damper combination. From this simple subsystem a damping coefficient can be determined that reduces the typical vibrations supercritical. Since damping in ligaments and contact descriptions has too little influence, an extra damper element is added. In simulations the fibula bounces against the tibia in lateral direction and is therefore responsible for vibrations found in tibia F_y force. An extra damper element is added with a damping coefficient ranging from 50 to 2000 kg s^{-1}. As a result many of the vibrations disappear, but only in a lateral direction. Also the kinematics of the ankle changes significantly, reducing biofidelity.

- A drastic solution to reduce fibula to tibia bouncing is fixing them together. This results in locking up of the ankle joint in inversion/eversion rotational direction and causes the fibula to transmit axial forces of the same order as the tibia, which is not considered biofidelic.

This leads to the conclusion that vibrations disrupt many of the global response signals, but that any solution has drawbacks or little effect; damping in contacts and ligaments has little influence, nodal damping is not physical and bone fixation disrupts ankle kinematics. No solution is presented here, so the signals that are being used for evaluation of the model need a comment on these vibrations.

8 Injury Prediction

The main aim of the currently developed model is to predict injuries. From the discussion in paragraph 9.1and 9.2 it can be concluded that the model's global behaviour is of sufficient quality to concentrate on the local behaviour.

In chapter 3 the injuries that are most often inflicted to the lower leg under frontal impact conditions were discussed. The underlying injury mechanisms should be simulated correctly. Also an experimental validation set for injury prediction is available, since three of the UVa experiments, discussed in chapter 6, inflicted injuries. But first a good definition of injury in terms of force, stress or strain is required. For a discussion on injury prediction it is referred to paragraph 9.3.

8.1 Injury Parameters

In the current model the discrete mesh provides local data for all bone parts of long bones and hindfoot. These local data consist of nodal forces, both internal and external, and of calculations of stresses and strains in elements.

The external nodal forces are generated by multibody contact algorithms or by ligaments and muscles connected to the nodes. The discrete force distribution over the bone mesh provides insight in the load paths in the bones and can hence localise possible injuries. The external forces, acting upon the nodes of elements, generate stresses and strains in these elements. The stresses and strains may also function as an indicator for injury.

In reality two types of bone failure need to be distinguished: shear and crush fractures. Shear fractures occur at stress concentrations caused by non-axial forces acting upon an element. Crush fractures occur as a consequence of hydrostatic pressure in the bone tissue. In continuum mechanics theory, the Cauchy stress tensor can be subdivided in a hydrostatic part and a shear part:

$$\sigma = \tfrac{1}{3} tr(\sigma) \boldsymbol{I} + \sigma^d \qquad (8.1)$$

In this equation the trace of the stress tensor $tr(\sigma)$ represents the hydrostatic part, while the deviatoric part of the tensor σ^d represents shear forces.

The finite element code uses the Von Mises stress for its yield criterion, which is defined by:

$$\sigma_v = \sqrt{-3J_2^d} = \sqrt{\frac{3}{2} tr(\sigma_d \cdot \sigma_d)} \qquad (8.2)$$

Since the deviatoric part of the Cauchy stress tensor is used in equation (8.2), the Von Mises stress is a measure of shear failure, and as a consequence excludes effects of volume change [Claessens, 1997]. Thus can be concluded that the criterion used in the code does not predict crush injuries. The injury tolerance for crush should alternatively be defined by the first principal stress σ_1 or the trace of the principal stresses.

Material failure occurs when the calculated Von Mises stress exceeds the defined yield stress. Since this is a good criterion for shear injuries only, an adaptation of the yield criterion should be made for crush injuries. The latter injuries are most likely to occur at ankle pilon, talus and calcaneus, whereas shear injuries occur in long tibia and fibula, malleoli and calcaneus. It appears that in crush type material failure, the first principal stress is higher than the Von Mises stress. In contradiction, for shear material failure the Von Mises stress is generally higher than the first principal stress. Generally the yield stress can be a good indicator of material failure, but the plastic behaviour occurring afterwards is chosen arbitrarily, therefore no post-fracture responses should be considered.

8.2 Load Paths

Simulating the load paths through the lower leg requires a force distribution corresponding with the real life situation. In the figures below the force distribution in an axial loading experiment is depicted together with anatomical drawings of corresponding articular surfaces.

The figures shows that the majority of nodal forces coincide with the articular surfaces. The force is sometimes too much concentrated on a small amount of nodes. This is due to the discrete mesh, where the jagged curves introduce local nodal intrusions. It should also be noted that the simulated articular surface of the calcaneus lies too far to the posterior side.

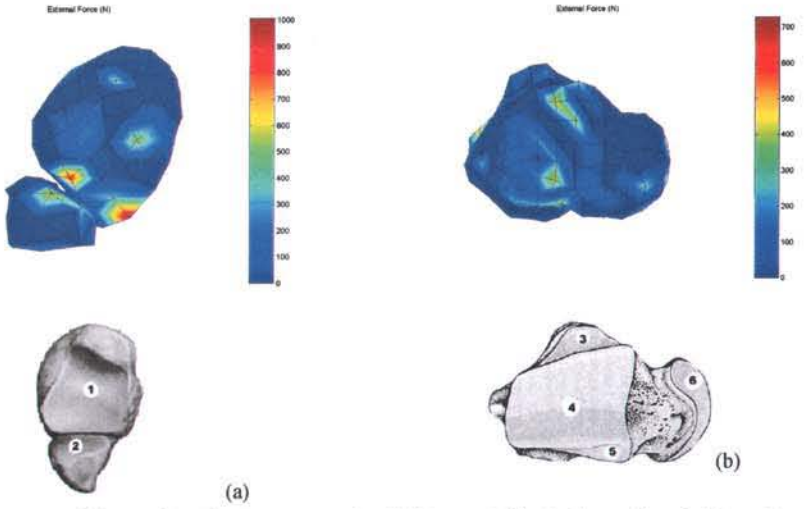

Figure 8.1: external force distribution at mesh of tibia and fibula from distal (a) and proximal talus (b) compared to the anatomical location of articular surfaces. Anterior is to the right in all cases.

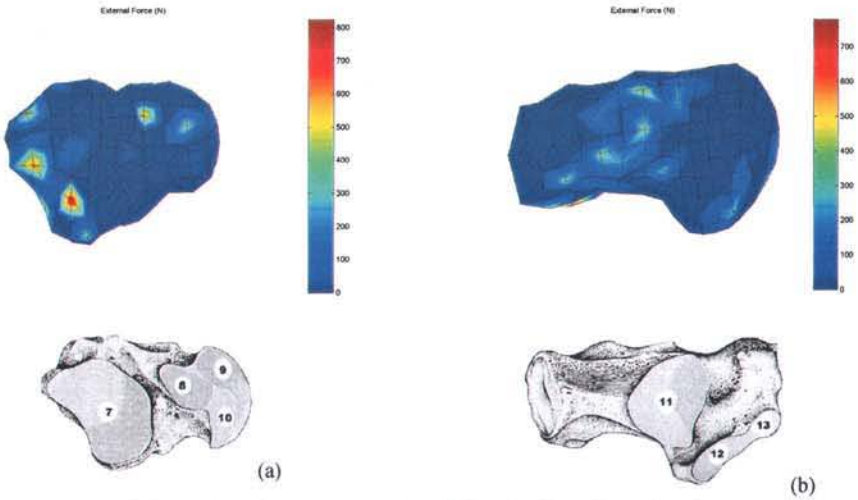

Figure 8.2: external force distribution at mesh of distal talus (a) and calcaneus (b) compared to the anatomical location of articular surfaces. Anterior is to the right in all cases.

8.3 Correlation with Injury Mechanisms

The most important injury mechanisms are axial loading, dorsiflexion, inversion and eversion loading, as described in chapter 3. Simulations with various boundary conditions are executed. For axial loading simulations the standard UVa experiments can be used. For the simulation of dorsiflexion the TRL toe impact tests are used. For inversion and eversion simulation UVa experiment 5c is used, with an additional footplate rotation around its longitudinal axis.

8.3.1 Axial Impact

The force distribution upon axial impact is shown and discussed in the former paragraph. The stress distribution is shown in Figure 8.3 and Figure 8.4. High bending stresses appear in the tibia diaphysis on the lateral side and in proximal talus and calcaneus. The occurrence of high stress generally corresponds to locations of high pressure, except for the tibia diaphysis where bending stresses occur.

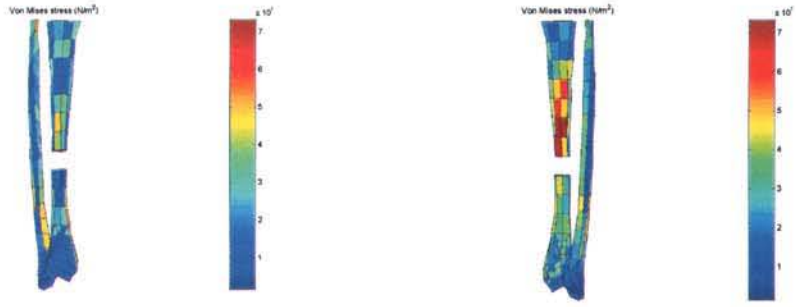

Figure 8.3: Von Mises stress distribution over the tibia and fibula from medial (l) and from lateral (r).

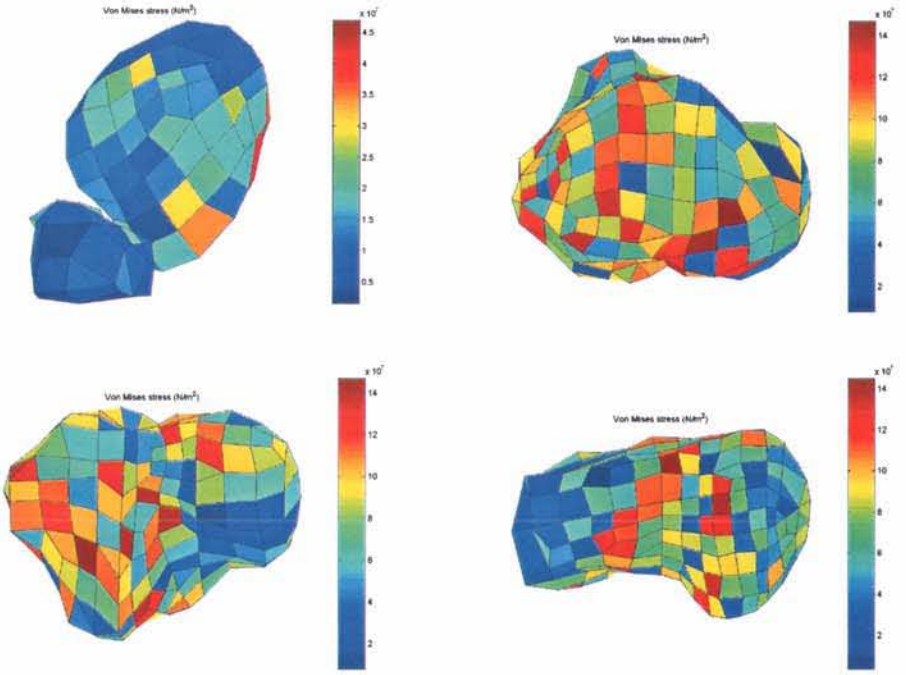

Figure 8.4: Von Mises stress distribution over the following bone parts: tibia and fibula from distal (top left), talus from proximal (top right), talus from distal (bottom left) and calcaneus from proximal (bottom right). Anterior is to the right in all cases.

In three UVa axial impact experiments failure has occurred. No information is provided on the time instant, but it can reasonably be assumed that failure occurs at the moment of maximum tibia axial force. As shown in Figure 6.7 the force and time instant at which failure occurs do not always correspond with the model.

The reported failures from experiments are as follows:

5c: extra-articular oblique calcaneus shear fracture on the medial side
5d: intra-articular calcaneus crush and a chip on the lateral side of the talus
7d: open tibia pilon fracture, crush of the lateral malleolus and a tibia plateau fracture

The simulation showed for all experiments a failure of both talus and calcaneus, of which no figures are shown. The talus is subject to crush along its main proximal articular surface (no. 4 in Figure 8.2). The calcaneus is subject to failure at the lateral edge of its main load bearing articular surface (no. 11 in Figure 8.2). Since Von Mises stress and first principal stress are equal, the failure is assumed to be of a combined crush and shear type.

8.3.2 Dorsiflexion

The dorsiflexion experiment is shown in Figure 8.5. The simulation shows that upon toe impact the tarsals press against the talus, forcing it to move in posterior direction. As a results the talus slides backwards along the tibia articular surface.

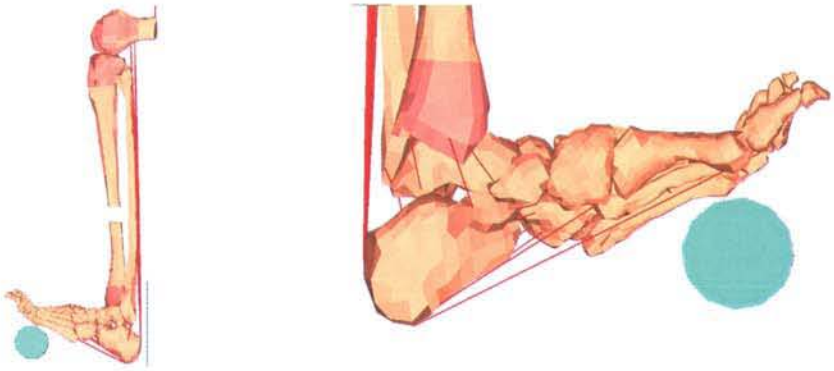

Figure 8.5: dorsiflexion simulation from lateral (l) and medial (r) viewpoints

The force distribution plot of the talus from a distal viewpoint is shown below. Compared to Figure 8.2c the force is more concentrated on the anterior side of the talus. Only a slightly increased load can be deduced at the most anterior articular surface on the distal side of the talus. This force is induced by the navicular bone of the forefoot. No significant differences in the stress distribution can be found here compared to axial impact.

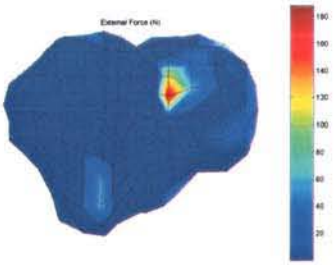

Figure 8.6: forces on distal talus in dorsiflexion simulation

8.3.3 Inversion and Eversion

Inversion and eversion experiments are shown in Figure 8.7. The rotated footplate induces a rotation of the forefoot along its longitudinal axis. In reality the contact between talus and malleolus may cause injury, but simulations do not show these contacts. Furthermore the calcaneus is reluctant to rotate.

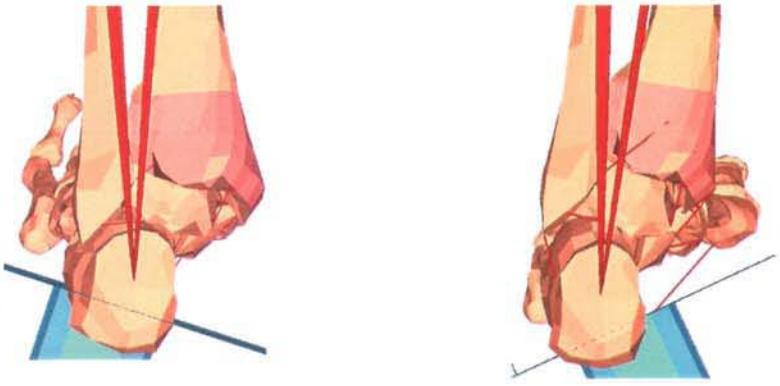

Figure 8.7: simulations of eversion (l) and inversion (r) as seen from the back of the foot

Comparing the load paths from inversion and eversion simulations with the experimentally determined force distribution on the proximal talus [Calhoun, 1994], we find similar force areas on the articular surface.

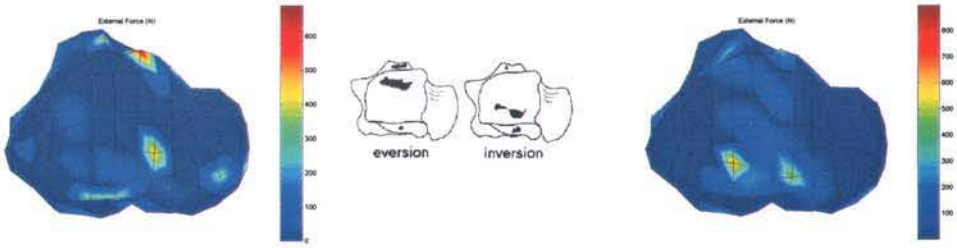

Figure 8.8: comparison of forces applied to proximal talus mesh and experimentally observed pressure distributions in eversion (l) and inversion (r)

9 Discussion

9.1 Model Evaluation

The results, as presented in chapter 6, are subject to discussion since they function as an evaluation of the biofidelity of the model. Differences between experiment and model response are attributed to either limitations of the model itself or to uncertainties concerning the boundary conditions.

Input signal
At first footplate acceleration resulting from the pendulum impact in UVa tests is used as the input signal for the model. Acceleration peaks range from 25 g to 340 g with an accompanying displacement from 15 mm to 85 mm. This boundary condition is therefore exactly the same in both experiment and model. For experiment 6i and 7d muscle pretension is applied. The consequences of the boundary condition difference explained in paragraph 6.1.2 will be discussed below.

External forces
The external forces the lower leg applies to the test setup consist of a footplate force, a kneeplate force, a femur load bolt force and in two cases an Achilles preload force. Foot- and kneeplate axial force are a direct consequence of the impact. Foot- and kneeplate forces in x- and y-direction are fully dependent on friction between skin and foam, but they show too many vibrations to be able to compare them. Moments measured in both plate loadcells are strongly dependent of the relative position of the foot with respect to the load cells. Since the positioning of the foot on the loadcell is not accurately known, moments should not be compared. Also the discrepancy in Achilles modelling does not allow for a comparison of external forces in muscle pretension experiments.

Ankle rotations
Three ankle rotations are defined by the relative orientation of the two accelerometer cubes fixed to tibia loadcell and metatarsals. This accurate positioning allows for a valid ankle rotation comparison. The dorsiflexion angle is clearly overpredicted by the model. Simulations show that the heel of the foot sinks deep into the foam, whereas the ball of the foot does not. This problem can be attributed to either too low foam stiffness or to too little ankle dorsiflexion resistance.

For TRL toe impact tests the dorsiflexion angle is higher than unaware volunteer tests show. Since foam intrusion plays no role here, the only remaining conclusion left is that the model ankle joint shows too little resistance to dorsiflexion.

Both experiment and model show eversion as a natural response of the ankle joint upon axial loading. After a longer period of time the ankle rotates towards

inversion in both simulation and model for severe impact loading experiments 5c, 5d and 7d. These experiments all incorporated bone failure and since the model does not predict post-fracture response no conclusions can be drawn on this effect.

The rotation around the z-axis of the ankle joint induces an internal or external rotation of the foot. From all five experiments a large range in rotations appears, whereas the simulation shows internal rotation throughout.

Tibia loadcell

In the tibia loadcell one axial force F_z, two shear forces F_x and F_y and two moments M_x and M_y are measured.

Axial force

Tibia loadcell signals are at first characterised by an initial value, caused by the clamping of foot- and kneeplate. A striking fact here is that for all simulations without muscle pretension tibia axial force is zero at time zero. Apparently force relaxation has occurred during the quasi-static clamping phase of 100 ms, given the fact that at first tibia axial forces were measured. The initial tibia axial force is overestimated by the simulations in cases with muscle pretension. This is caused by the difference in muscle pretensioning method, as discussed before.

The general response in tibia axial force is further characterised by one peak load, resulting from the first footplate acceleration pulse. All peak loads, except for 5c and 7d, approximate the experimentally observed values. In the latter case, this is due to an exceeded yield stress in the simulation, whereas the used PMHS is of an extraordinary strong kind, compared to that of other experiments (see Table D.1). Apparently the specimen used in experiment 5c was of a weaker kind, since early failure occurred.

Shear forces

The forces in x- and y-direction are indicators of shear in the tibia. Both experiment and simulation indicate shear forces in positive x-direction, thus applying anterior shear to the distal tibia. For experiments 5c, 5d and 7d tibia F_x force is higher than found in experiments, caused by a bending failure of the distal tibia around 25 ms. Tibia force in y-direction corresponds to a rightward shear of the distal end of the foot. For both experiment and simulation there is no consistency between signals as they fluctuate around zero. The mechanism behind the occurring tibia shear and the possible cause, eversion of the ankle, is not yet fully understood.

Moments

The moments measured in the tibia loadcell are very much dependent on the orientation of the tibia loadcell with respect to the tibia. At both UVa and TRL procedures are used for loadcell placement, but they have not been reproduced with accuracy in the simulation environment. In the experimental setup no trend is found in occurring moments due to axial impact. Since eversion shows as a natural

response in all experiments, an eversion moment is expected. Still only in 2 out of 5 cases this shows. All simulation signals show an eversion moment, but again it should be noted that no conclusions should be drawn from this. The tibia moment around the y-axis is defined as a dorsiflexion moment. In all simulations this signal fluctuates around zero, where it is referred to paragraph 7.5.

Accelerations
The TRL pendulum acceleration upon impact to the ball of the foot evaluates the model used for plantar tissue and the dorsiflexion movement of the ankle joint. The curve is characterised by a peak and a subsequent plateau. The peak is well described by the model if compared to a PMHS test, but too small compared to volunteer tests. The peak evaluates the elasticity of the contact between the rigid impactor and the plantar tissue. Apparently in vivo plantar tissue is stiffer than PMHS plantar tissue, presumably caused by the water constituent of the biphasic tissue. The acceleration plateau is merely a measure of hysteresis of plantar tissue and of the resistance to dorsiflexion of the ankle joint. Since the simulation shows a bouncing effect of the pendulum, too small energy absorbence of plantar tissue and low resistance to dorsiflexion appear in the model.

9.2 Parameter Sensitivity

From the parameter sensitivity study executed in chapter 7 it appears that the parameters concerning the bone finite element description should be handled with care. The shell element description entails severe simplifications that are not easily described by experimentally determined parameters. As far as the parameters from the multibody components are concerned, these are found to be insensitive to variations within the ranges defined in literature.

The parameter study that is executed as a possible solution to the non-physical occurrence of vibrations in global response signals is unsuccessful so far. It has been impossible to find a compromise that reduces vibrations without losing the biofidelity of the model.

9.3 Injury Prediction

The aim of the currently developed model is the capacity to predict injuries. In chapter 8 the results on this investigation are presented. This leads to the following discussion.

The bone mesh is generally of sufficient quality to replicate the articular surfaces found in real bone parts. Most of the load paths are found to run through these surfaces. Still, concentrated forces are exerted on the nodes, caused by the jagged curves that describe the mesh. A smoother mesh, with more elements, would allow a better replication of the articular surfaces.

The ankle joint of the model shows that it can simulate the change of load paths under different loading conditions, especially inversion and eversion.

The stress distribution often corresponds to the distribution of external forces over the mesh. Also bending stresses in long bones show up well. In turn large gradients between computed stresses in surrounding elements turn up, as Figure 8.3 and Figure 8.4 show. This is also due to mesh coarseness, where jagged edges and few integration points induce high stress gradients. A refined mesh would show a more detailed stress distribution, which improves the chances of good injury prediction.

Furthermore it appears that the results of injury mechanism experiments are very much dependent on the boundary conditions of the experiment. For example the inversion experiment does not show medial malleolus contact, whereas an experiment can be thought of where the calcaneus is fixed to the footplate, thus inducing more calcaneus rotation without sliding downward of the footplate. Also obvious differences exists between a footplate dorsiflexion test and the executed toe impact experiment. In the latter test force is only applied to the ball of the foot, thus inducing more pressure on the anterior talus.

Concerning the use of different stress measures for different loading types, the deviation between Von Mises stress and first principal stress needs discussion. For shear failure experiments the yield stress functions as a good injury predictor, since Von Mises is a typical shear criterion. In crush type failure, the first principal stress should be used as an injury predictor, whereas the code always uses Von Mises stress as a criterion. Since in crush type failure the first principal stress is generally 20 MPa higher than the Von Mises stress, a 15% error is made in the prediction of injury.

A comparison of the regions where yield stress was reached with the reported failures from UVa experiments shows a correlation for calcaneus and talus. Since a wide range of injuries have occurred in three comparable experiments, the exact location of injuries upon axial impact is hard to simulate. Therefore the chosen combination of Young's modulus, yield stress and element thickness for separate bone parts is not validated by this injury occurrence correlation.

Since the yield stress functions merely as a measure of failure in the current model, no conclusions can be drawn on the plasticity of the material after reaching the yield value. Also global responses from chapter 6 should not be considered valid after yielding occurred.

From the model it seemed that the ligaments did not induce injuries to bone parts, since no high external forces are found at the nodes where the ligaments were attached. Also no ligament failure is incorporated in the model, since that is considered of less importance in literature.

With the current model no statements can be made on the injury tolerances discussed in paragraph 3.3. The occurrence of injuries can be predicted under different loading conditions, but no quantitative measures can be given on angles or maximum forces. Again this might be due to mesh coarseness and the resulting stress irregularities.

10 Conclusions and Recommendations

The present study involves the development of a numerical human lower leg model that can be used as research tool for injury prediction. The model consists of a finite element mesh description interconnected by multibody kinematic ligaments, muscles and contact descriptions. The constitutional behaviour of all tissues complies with experimentally observed ranges under comparable circumstances.

Model evaluation
From the evaluation of the global response of the model against experimental data the following can be concluded:

In general, simulated axial forces show good correspondence with experimental loadcell measurements. The peak force is simulated with at most 10% deviation, except for experiments where failure occurred. The moment of failure is too much dependent on the physical properties of the PMHS and can therefore not be correctly simulated for all cases;

Axial forces measured in foot- and kneeplate can not be compared for experiments with muscle pretension, caused by the difference in Achilles boundary condition modelling;

Forces in lateral and longitudinal direction and loadcell moments show poor correlation. At first the exact location and orientation of loadcells is unknown and secondly the non-physical vibrations disturb these signals to a more serious extent than the axial forces;

Considering ankle kinematics the structure of the ankle joint in the model proves to be of sufficient quality to replicate dorsiflexion, inversion and eversion rotations. The bone mesh, cartilage contact characteristics and ligaments make up an ankle joint that is stable under severe impact conditions and that constitutes the natural kinematics. The latter means that the ankle joint has a tendency to evert under axial impact and that it simulates dorsiflexion, inversion and eversion experiments to a satisfactory extent;

Furthermore the global response of the model to both UVa and TRL simulations proves that the model can be applied for different levels of impact. The most important signals, like tibia axial force and ankle rotation, are well described by the model in a range of impact from 30 g to 350 g;

As a result the developed model has a satisfactory degree of biofidelity on a global level, although not all global signals can be used for validation purposes. Furthermore the model is robust, since it is stable under all conditions, except for the post-injury response, which is not discussed after all. Since the global

characteristics of the model correspond to experimental data, a closer look at local information for injury prediction purposes is allowed.

Injury prediction

The developed model, which shows sufficient biofidelity on a global level, is evaluated for its injury prediction application. The following conclusions can be drawn:

The analysis of load paths shows that the external nodal forces are exerted on the mesh of the different bone parts at locations corresponding to the articular surfaces of real bones. Hence the load path prediction upon axial impact is correctly simulated by the model. Nevertheless due to mesh coarseness forces are sometimes too much exerted on a single node, not carefully describing the smooth articular surface;

A change in load path is shown for inversion and eversion experiments and validated against experimentally observed pressure distributions on the proximal talus articular surface. For dorsiflexion experiments a change in load path does not show so clearly, although differences do occur in TRL toe impact tests;

Failure is incorporated in the model by a yielding value in the elastoplastic material model for bone. Since only a small sample of experimental data with failure is available, no extensive conclusions can be drawn. Experimentally observed failure partially corresponds to simulated failure, which manifests in talus and calcaneus crush. In addition tibia failure is observed experimentally, whereas it does not occur in the simulation, although tibia loadcell axial force shows good correlation;

In the current model it is impossible to draw conclusions from stress distributions over the bone mesh. Due to mesh coarseness, the stress distribution shows too large gradients with surrounding elements. Although failure is predicted correctly under axial impact, no information is provided for injury locations in the other most occurring injury mechanisms;

Summarising it appears that the lower leg model shows a capacity to simulate load paths under the most often occurring circumstances, rather than transmit forces through a single kinematic spherical joint. The stress distribution shows irregularities, due to mesh coarseness, but it can localise injuries by a correct definition of the yielding threshold;

It should further be noted here that this model is, as far as literature references go, the first numerical human lower leg model that simulates load paths under different loading conditions. Also the correlation with experimentally observed injuries has never been simulated before.

Recommendations

From the conclusions drawn before, a number of recommendations for further research can be made:

Resulting from the global response signals, further research should be done on the non-physical occurrence of vibrations. The problem is investigated in this thesis, but only to a certain extent and without a satisfactory result. The lower leg model should be divided in different sections. The dynamics of all sections should then be separately investigated, including the interactions between sections;

If the model will be used for research purposes in the future, efforts should be made to reduce computational time. Since no deformation and stress behaviour in the femur is considered, this mesh might be turned into a multibody description. Also the search algorithms for contacts between elements and nodes can be speeded up. In the current model, algorithms search for interactions between nodes and elements that will never contact each other, like proximal tibia with talus contact;

Since no satisfactory conclusions are drawn from provided information on stresses in elements, the FE mesh should be further improved. The influence of mesh refinement on the stress distribution needs investigation, since large stress gradients are thought to disrupt the stress distribution. Furthermore, jagged edges are thought to induce stress concentrations. Thus besides a multiplication of the number of elements also a smoothing procedure of the mesh should be executed. It should be noted that this is in contradiction with the former proposed reduction of computational time;

As a consequence of an insufficient stress analysis no predictions of injury tolerances can be made with the current model, which is an important part of a model with injury prediction capabilities. In further research the FE parameters should be found that induce yield stresses at reported failure forces, moments and rotation angles;

A reduction of computational time becomes of major importance if the lower leg model is to be used for car safety design purposes. In that case each bone part will be transformed into a multibody mesh and then subdivided in a small amount of bodies. Each body will be responsible for transmitting a part of the total impact force, depending on the load path. The deformation of the bone part is then lumped into the joints that connect the different bodies. Here injury tolerances can be defined, not in terms of experimentally observed injury tolerances, but in terms of local information, like load path force and stress.

References

- ADRIA report (1998) Test Set-up Description and Description of Injury Mechanisms of Car Occupants in Frontal Collisions, Deliverable D10
- Artis, M.; McDonald, J.; White, R.; Huang, T.J.; Shams, T.; Rangarajan, N.; Akiyama, A.; Okamoto, M.; Yoshizawa, R.; Ishikawa, H. (2000) Development of a New Biofidelic Leg for Use with a Pedestrian Dummy, IRCOBI conference paper, Montpellier, France, September 20th-22nd 2000
- Attarian, D.E.; McCrackin, H.J.; DeVito, D.P.; McElhaney, J.H. Garrett, W.E. (1985) Biomechanical Characteristics of Human Ankle Ligaments, Foot & Ankle, Vol. 6, N°2, Oct. 1985
- Beaugonin, Muriel; Haug, Eberhard; Munck, Grégoire (1995) A Preliminary Numerical Model of the Human Ankle Under Impact Loading, PLEI Conference, Washington D.C.
- Beaugonin, Muriel; Haug, Eberhard; Munck, Grégoire; Cesari, Dominique (1996) The Influence of Some Critical Parameters on the Simulation of the Dynamic Human Ankle Dorsiflexion Response, 96-S10-W-31, 15th ESV Conference, Melbourne, Australia, May 13-17, 1996 [1]
- Beaugonin, Muriel; Haug, Eberhard; Cesari, Dominique (1996) A Numerical Model of the Human Ankle/Foot Under Impact Loading in Eversion and Inversion, SAE paper [2]
- Beaugonin, Muriel; Haug, Eberhard; Cesari, Dominique (1997) Improvement of Numerical Ankle/Foot Model: Modelling of Deformable Bone, Society of Automotive Engineers, SAE paper 973331
- Bedewi, Paul G.; Marzougui, Dhafer M. (1998) Finite Element Modelling of Fracture in Long Bones, FHWA/NHTSA National Crash Analysis Centre, The George Washington University, Ashburn, Virginia, USA
- Begeman, Prasad (1990) Human Ankle Impact Response in Dorsiflexion
- Begeman, P.; Balakrishnan, P.; Levine, R.; King, A. (1993) Dynamic Human Ankle Response to Inversion and Eversion, Proceeding 37th Stapp Car Crash Conference, San Antonio, Texas, 1993, pp.83-93
- Begeman, P.; Paravasthu, N. (1997) Static and Dynamic Compression Loading of the Lower Leg, Proc.7th Injury Prevention Through Biomechanics Symposium
- Behrens, J.C. et al. (1974) Variation in Strength and Structure of Cancellous Bone at the Knee, J. Biomech 7:201-207
- Beillas, Phillippe; Lavaste, François; Nicolopoulos, Dimitri; Kayventash, Kambiz; Yang, King H.; Robin, Stéphane (1999) Foot and Ankle Finite Element Modelling Using CT-Scan Data, 43rd Stapp Car Conference Proceedings
- Bojsen-Møller, F.; Flagstad, K.E. (1976) Plantar Aponeurosis and Internal Architecture of the Ball of the Foot, Journal of Anatomy, 121(3), 599-611
- Burghele, N.; Schuller, K. (1968) Die Festigkeit der Knochen Kalkaneus und Astragllus. Aus der Klinik fur Orthopädie des Bukarester Unfallkrankenhauses

und dem Lehrstuhl fur Festigkeit und Materialprufungswesen der Technischen Hochschule, Bukarest, Rumännien (in German)
- Burstein, A.H. et al. (1976) Aging of Bone Tissue: Mechanical Properties, J Bone Joint Surg 58(A):82
- Calhoun, Jason.H.; Fan Li; Ledbetter, Billy R.; Viegas, Steven F. (1994) A Comprehensive Study of Pressure Distribution in the Ankle Joint with Inversion and Eversion, Foot & Ankle 15(3), 125-133
- Cappon, H.J.; Kroonenberg, R.; Happee, R.; Wismans, J.S.H.M. (1999) An Improved Lower Leg Multibody Model, Proceedings of IRCOBI conference, Sitges, Spain, September 1999
- Carothers, C.O. et al. (1949) The Elasticity and Strength of Some Long Bones of the Human Body, Naval Med Research Inst, Project NM, 001, 056.0213
- Carter, D.R. et al. (1977) The Compressive Behaviour of Bone as a Two-Phase Porous Structure, J Bone Joint Surgery 59A:954-962
- Ciarelli, M.J. et al. (1986) Experimental Determination of the Orthogonal Mechanical Properties, Density, and Distribution of Human Trabecular Bone from the Major Metaphyseal Regions Utilising Material Testing and Computed Tomography, Trans Orthop Res Soc, p42, 1986
- Ciarelli, M.J. et al. (1991) Evaluation of Orthogonal Mechanical Properties and Density of Human Trabecular Bone from the Major Metaphyseal Regions with Materials Testing and Computed Tomography, J Orth Res 9:674-682, 1991
- Claessens, Maurice H.A. (1997) Finite Element Modelling of the Human Head under Impact Conditions, Ph.D. report, Eindhoven University of Technology, Eindhoven, The Netherlands
- Crandall, J.R.; Martin, P.G.; Sieveka, E.M.; Klopp, G.S.; Kuhlmann, T.P.; Pilkey, W.D.; Dischinger, P.C.; O'Quinn, T.D.; Schmidhauser, C.B. (1995) The Influence of Footwell Intrusion on Lower Extremity Response and Injury in Frontal Crashes, 39th annual proceedings of ass. for the advancement of aut. med.
- Crandall, J.R.; Kuppa, S.M.; Klopp, G.S.; Hall, G.W.; Pilkey, W.D.; Hurwitz, S.R. (1997) Injury Mechanisms and Criteria for the Human Foot and Ankle under Axial Impacts to the Foot, 21-11-1997, IJCrash Vol. 3, No. 2
- Davis, W.H. et al. (1996) Gross, Histological, and Microvascular Anatomy and Biomechanical Testing of the Spring Ligament Complex, Foot & Ankle International
- Ducheyne, P et al. (1977) The Mechanical Behaviour of Intracondylar Cancellous Bone of the Femur at Different Loading Rates, J. Biomech 10:747-762
- Evans, F.G. et al. (1951) Regional Differences in Some Physical Properties of Human Femur, J Appl Physiol 3:563-572
- Fung, Y.C. (1981) Biomechanics: Mechanical Properties of Living Tissues, Springer-Verlag, New York, NY
- Funk, James R.; Hall, Gregory W.; Crandal, Jeff R.; Pilkey, Walter D. (1998) Linear and Quasi-Linear Viscoelastic Characterization of Ankle Ligaments, Revision

- Funk. James R (2000) Summary of Available Data from UVa Cadaver Lower Extremity Axial Impact Tests, UVa document, University of Virginia, Charlottesville (VA), USA
- Furusu, Katsuya; Iwamoto, Masami; Miki, Kazuo; Kato, Chiharu; Hasegawa, Junji (1999) Development and Validation of the Finite Element Model of the Human Lower Extremity for Accidental Injury, SAE paper 9934582
- Goldstein, S.A. et al. (1983) The Mechanical Properties of Human Tibia Trabecular Bone as a Function of Metaphyseal Location, J Biomech 16:965-969
- Hall, Gregory W. (1998) Biomechanical Characterization and Multibody Modelling of the Human Lower Extremity, Dissertation University of Virginia, May 1998
- Hill, A.V. (1938) The Heat of Shortening and the Dynamic Constants of Muscle, Proc. R. Soc. Lond. 126: 136-195
- Hori, R.Y.; Mockros, L.F. (1976) Indentation Tests of Human Articular Cartilage, Dep. Civil Engineering, Northwestern University, Evanston, USA, J.
- Hvid, I. et al. (1985) Trabecular Bone Strength Patterns at the Proximal Tibial Epiphysis, J orthop Res 3:464-472.
- Inman, V.T. (1976) The Joints of the Ankle, Baltimore, MD, Williams and Wilkins, p. 27
- Kimura, H. (1952) Tension Test Upon the Compact Substance in the Long Bones of Cattle Extremities, J Kyoto pref Med Univ 51:365-372
- Kitagawa, Yuichi; Hideaki, Ichikawa; Pal, Chinmoy; King, Albert I.; Levine, Robert S. (1998) Lower Leg Injuries Caused by Dynamic Axial Loading and Muscle Tensing
- Lawson, A.R.; Payne, A.R.; Clemo, K.C. (1998) An Understanding of the Mechanisms of Lower Leg Injuries from Accident Data and Crash Testing, MIRA, UK
- Ledoux, William R.; Meany, David F.; Hillstrom, Howard J. (1999) A Quasi-Linear, Structural Model of the Plantar Soft Tissue With Frequency Dependent Damping Properties, 23rd Annual Meeting, American Society of Biomechanics
- Lestina, Diane C.; Kuhlmann, Thomas P.; Keats, Theodore E.; Alley, Maxwell R. (1992) Mechanisms of Fracture in Ankle and Foot Injuries to Drivers in Motor Vehicle Crashes, SAE paper 922515
- Lewis G.; Shaw K.M. (1997) Tensile Properties of Human Tendo Achillis: Effect of Donor Age and Strain Rate, J Foot Ankle Surg 1997 Nov; 36(6): 435-445
- Lindahl, O. (1976) Mechanical Properties of Dried Defatted Spongy Bone, Acta Orthop Scand 47:11-19
- Linde, F. et al. (1989) Energy Absorptive Properties of Human Trabecular Bone Specimens During Axial Compression, J Orth Res, 7:432-439
- Manning, Paul; Wallace, Angus; Owen, Clare; Roberts, Adrian; Oakley, Charles; Lowne, Richard (1998) Dynamic Response and Injury Mechanism in the Human Foot and Ankle and an Analysis of Dummy Biofidelity, paper 98-s9-O-11, TRL, United Kingdom

- McElhaney, D.A. et al. (1970) Mechanical Properties of Cranial Bone, J Biomech 3:495-511
- Meijer, R., Hoof, J. van, Happee, R., et al. (2001), Effects of Leg Bone Bending in Car-Pedestrian Impact Evaluated Using a Finite Element Human Leg Model, confidential TNO report 01.OR.BV.008.1/RME, 2001
- Morgan, Richard M.; Eppinger, Rolf H.; Hennessey, Barbara C. (1991) Ankle Joint Injury Mechanism for Adults in Frontal Automotive Impact, SAE paper 912902
- Morris, Andrew; Thomas, Pete; Taylor, Andrew M.; Wallace, W. Angus (1999) Mechanisms of Ankle and Hind-foot Injuries to Drivers and Passengers in Frontal Crashes as Deduced from Field Studies, 05-03-1999
- Mullender, Margriet G. (1997) The Process of Mechanical Adaptation in Trabecular Bone, Dissertation of Nijmegen Catholic University
- Niggs, B.M.; Skarvan, G.; Frank, C.B. (1990) Elongation and Forces of Ankle Ligaments in a Physiological Range of Motion, Foot & Ankle, Vol. 11 (1), pp. 30-40, 1990
- Oloyede, Adekunle; Flachsmann, Rene; Broom, Neil D. (1992) The Dramatic Influence of Loading Velocity on the Compressive Response of Articular Cartilage, Connective Tissue Research 27, 211-224
- Otte, D.; Rheinbaben, H. von; Zwipp, H. (1992) Biomechanics of Injuries to the Foot and Ankle Joint of Car Drivers and Improvements for an Optimal Car Floor Development, SAE paper 922514
- Parenteau, Viano (1996) MADYMO Models of the Human and Dummy Lower Limbs to Investigate Biomechanical Responses, IJCrash, 1996, Vol 1 No 4 [1]
- Parenteau, Viano, Lövsund, Tingvall (1996) Foot-Ankle Injuries: Influence of Crash Location, Seating Position and Age, Accid.Anal.and Prev., Vol. 28 No. 5 pp 607-617 [2]
- Parenteau, C.S.; Viano, D.C. (1996) Kinematics Study of the Ankle-Subtalar Joints, Journal of Biomechanical Engineering (submitted), 1996 [3]
- Parenteau, C.S.; Viano, D.C.; Petit, P.Y. (1998) Biomechanical Properties of Human Cadaveric Ankle-Subtalar joints in Quasi-static Loading, J. Biomech. Eng., Vol. 120, 1998, pp 363-376
- Pilkey, Walter D.; Sieveka, Edwin M.; Crandall, Jeff R.; Klopp, Gregory (1994) The Influence of Foot Placement and Vehicular Intrusion on Occupant Lower Limb Injury in Full-Frontal and Frontal-Offset Crashes
- Portier, Laurent; Petit, Philippe; Dômont, Alain; Trosseille, Xavier; Le Coz, Jean-Yves; Tarrière, Claude; Lassau, Jean-Pierre (1997) Dynamic Biomechanical Dorsiflexion Responses and Tolerances of the Ankle Joint Complex, SAE paper
- Pugh, J.W. et al. (1973) Elastic and Viscoelastic Properties of Trabecular bone: Dependence on Structure
- Reilly, D.T. et al. (1975) The Elastic and Ultimate Properties of Compact Bone Tissue, J biomech 8:395-405
- Sarrafian, S.K. (1983) Anatomy of the Foot and Ankle, Philadelphia, Lippincott

- Sedlin, E.D. et al. (1965) A Theological Model for Cortical Bone. In a Study of the physical properties of human femoral samples, Acta Orthop Scandinavica Spplementum 83
- Sedlin, E.D. et al. (1966) Factors Affecting the Determination of the Physical Properties of Femoral Cortical Bone, Acta Orthop Scandinavica 37:29-48
- Serre, T.; Brunet, C. (2000) HUMOS: Geometry Acquisition of a Seated Man, Official deliverable of task 2.1, HUMOS document
- Siegmund, Gunter P.; Brault, John R. (2000) Role of Cervical Muscles During Whiplash, in Frontiers in Whiplash Trauma, N. Yoganandan, F.A. Pintar (Eds.), IOS press
- Tannous, Bandak, Toridis, Eppinger (1996) A Three-Dimensional Finite Element Model of the Human Ankle: Development and Preliminary Application to Axial Impulsive Loading, SAE paper
- Thomas, Pete; Charles, John; Fay, Paul (1995) Lower Limb Injuries – The Effect of Intrusion, Crash Severity and the Pedals on Injury Risk and Injury Type in Frontal Collisions, SAE paper
- TNO Automotive (1999) MADYMO: Theory Manual Version 5.4, May 1999
- Tsuda, K. (1957) Studies on the Bending Test and Impulsive Bending Test on Human Compact Bone, J Kyoto Pref Med Univ 61:1001-1025
- Valiant, G.A. (1984) A Determination of the Mechanical Characteristics of the Human Heel Pad In Vivo, Ph.D. Dissertation, The Pennsylvania State University
- Vincentelli, R. et al. (1985) The Effect of Haversian Remodelling on the Tensile Properties of Human Cortical Bone, J Biomech 18 (3) : 201-207
- Williams, J.L. et al. (1982) Properties and an Anisotropic Model of Cancellous Bone from the Proximal Tibia Epiphysis, J Biomech Eng 104:50-56
- Yamada, H. (1970) Strength of biological materials, In Evans FG. (ed), Williams and Wilkins, Baltimore
- Yang, Yikuang (1998) HUMOS: Biomaterial Characterisation, Official deliverable of task 3.1, HUMOS document
- Yoganandan, Narayan; Pintar, Frank A., Boynton, Melbourne; Begeman, Paul; Prasad, Priya; Kuppa, Shashi M.; Morgan, Richard M.; Eppinger, Rolf H. (1996) Dynamic Axial Tolerance of the Human Foot-Ankle Complex, SAE paper
- Yokoo, S. (1952) The Compression Test Upon the Diaphysis and the Compact Substance of the Long Bones of Human Extremities, J Kyoto Pref Med Univ 51:291-313

Appendix A Injury Statistics

Besides the statistics from real world accidents, also investigations on the influence of certain parameters of injury risk were carried out. Below an overview is given of parameters that are considered important for lower leg injury prediction.

Influence of Intrusion

In many frontal car crashes intrusion of the footwell occurs. To be able to justify the importance of intrusion in real world lower leg injuries Crandall [Crandall, 1995] made a survey from the NASS data files from 1988 to 1993. Again only frontal impact conditions were considered and rollover cases were excluded. In this survey all cases where contact with the control panel occurred are excluded, since the effect of footwell intrusion is investigated.

From this survey it can be concluded that the majority of injuries occur at a low intrusion level. Of a total number of 627 AIS 2+ injuries 60.7 % occurred in cases with almost no intrusion as Figure A.1a shows. Figure A.1b is derived from a much smaller sample from the NASS database. The location of fracture is determined from 76 AIS 2+ lower leg injury cases. Although this sample is too small to draw statistically valid conclusions a trend can be observed. In general most injuries occur along the load path from knee to heel. In case of severe intrusion more fractures tend to occur in the foot. Apparently the tarsals and metatarsals become trapped in the footwell compartment.

The occurrence of injuries in real world accidents determines the relative importance of different local injuries. A different approach is followed by Thomas [Thomas, 1995], who investigated the risk of obtaining an AIS 2+ injury from the UK CCIS files. It is concluded that the risk is about 3% for intrusion levels up to 10 cm, around 25% for medium intrusion levels, from 11 to 40 cm and up to 45% for intrusion levels higher than 40 cm, which contradicts Crandall's findings.

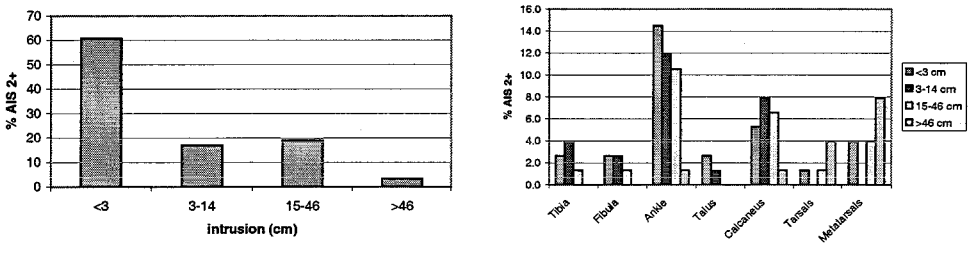

(a) (b)

Figure A.1: the influence of intrusion on the occurrence of AIS 2+ injuries (a) and the localisation of AIS 2+ injuries as a consequence of a frontal impact with a certain level of intrusion (b) [Crandall, 1995]

Influence of Delta-V

The difference in speed between two impacting objects, referred to as delta-V, is often regarded as a measure for crash severity. Many research has been conducted on determining the influence of this parameter on the probability of injuries. Investigations from Otte [Otte, 1992] and Morgan [Morgan, 1991] result in approximately the same probability risk function, as Figure A.2 shows. Thomas' research, based on data from the CCIS files from 1983 to 1995, resulted in a lower injury risk as a function of delta-V. Currently no explanation can be given on the deviation between different investigations. Although all data are derived from different databases, they meet the same boundary conditions. The risk function specified by Thomas is less plausible, since the other two curves show such good resemblance.

At 10 km/h delta-V the probability of an AIS 2+ injury is almost zero according to all three investigations. At 20 km/h the chance is around 10 percent for Otte's and Morgan's research, while Thomas still indicates zero chance. At legislatory testing speed (50 km/h) the injury risk is predicted to be around 70 % and at EURO-NCAP testing speed (64 km/h) the risk increases to 85 %.

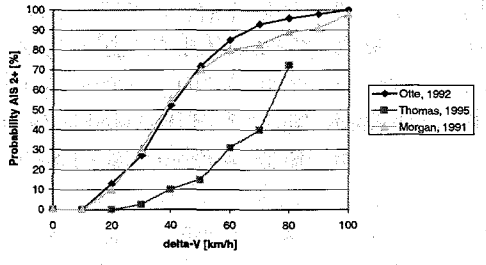

Figure A.2: Influence of delta-v on injury probability according to three different investigators

Influence of Age

The influence of age on injury possibility was first investigated by Yoganandan [Yoganandan, 1996]. From PMHS tests injury risk functions were defined for three different ages. Figure A.3 shows that the probability of injury increases with age if an axial dynamic impact load is applied. This age degeneration process is mainly due to changing tibia bone composition.

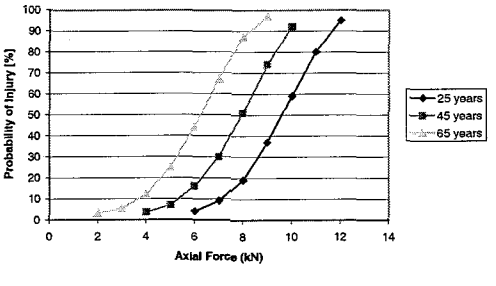

Figure A.3: Probability distribution for foot-ankle injury as a function of the dynamic axial force derived from PMHS tests for three discrete ages [Yoganandan, 1996]

Appendix B Material Properties

E (GPa)	Tension	Compression	Bending	Torsion	Unspecified
Femur **16.0**	**15.6-17.7** Burstein (1976) **13.5-14.6** Evans (1951) Wet **17.1-19.0** Evans (1951) Dry **17.3** Yamada (1970) Wet **20.2** Yamada (1970) Dry	**15.9-18.7** Burstein (1976) **26.7** Carothers (1949) **10.4** Kimura (10.4)	**15.8** Sedlin (1965) **15.5** Sedlin (1966)	**3.28** Reilly & Burstein (1975) **2.94-3.43** Yamada (1970)	**16.0** Meijer (2001)
Tibia **43.8**	**18.9-29.2** Burstein (1976) **19.7** Vincentelli (1985) **18.0** Yamada (1970) Wet **20.6** Yamada (1970) Dry	**24.5-35.3** Burstein (1976) **28.4** Carothers (1949)			**26.8** Meijer (2001) **43.8** Meijer (2001) modified **18.9** Bedewi (1998)
Fibula **43.8**	**18.5** Yamada (1970) Wet **21.1** Yamada (1970) Dry				**20.0** Meijer (2001) **43.8** Meijer (2001) modified
Talus **43.8**					
Calcaneus **43.8**	**0.284** Burghele and Schuller (1968)				

Table B.1: elastic modulus of different bones as determined by different authors under different loading conditions and as adopted for the model (left column)

σ_u (MPa)	Tension	Compression	Bending	Torsion
Femur	**120-140** Burstein (1976) **77-84** Evans (1951) Wet **99-111** Evans (1951) Dry **122** Yamada (1970) Wet **151** Yamada (1970) Dry	**179-209** Burstein (1976) **140** McElhaney (1970) **145-167** Yamada (1970) **159** Yokoo (1952)	**164** Sedlin (1965) **181** Sedlin (1966) **157** Tsuda (1957) **139-174** Yamada (1970)	**68** Reilly & Burstein (1975) **48.6-57** Yamada (1970)
Tibia	**145-170** Burstein (1976) **162** Vincentelli (1985) **140** Yamada (1970) Wet **170** Yamada (1970) Dry	**183-213** Burstein (1976)		
Fibula	**146** Yamada (1970) Wet **176** Yamada (1970) Dry			
Talus	**4591 N** Burghele and Schuller (1968) Dynamic			
Calcaneus	**2570 N** Burghele and Schuller (1968) Dynamic			

Table B.2: ultimate stress of different bones as determined by different authors under different loading conditions

Compression	E (MPa)	σ_u (MPa)
Distal femur **E = 13 MPa** **σ_u = 35 MPa**	**7.6-2942** Ciarelli (1986,1991) **413-1516** Pugh (1973) **13** Meijer (2001) **73.5** Yamada (1970)	**2.25-66.2** Behrens (1974) **19** Ciarelli (1986,1991) **0.98-22.5** Ducheyne (1977) **35** Meijer (2001)
Proximal tibia **E = 13 MPa** **σ_u = 30 MPa**	**1.4-79** Carter (1977) **8-457** Goldstein (1983) **4-430** Hvid (1985) **23.1-34.6** Lindahl (1976) **113-853** Linde (1989) **10-500** Williams (1982) **200** Meijer (2001) **1280** Meijer (2001) modified **73.5** Yamada (1970)	**1.8-63.6** Behrens (1974) **1.5-45** Carter (1977) **0.52-11** Ciarelli (1986,1991) **1-13** Goldstein (1983) **13.8-116.4** Hvid (1985) **2.2-3.9** Lindahl (1976) **1.5-6.7** Williams (1982) **20** Meijer (2001) **30** Meijer (2001) modified

Table B.3: mechanical properties of trabecular bone under compression according to different authors and as adopted for the model (left column)

σ_y (MPa)	Unspecified
Femur **120**	**120** Meijer (2001) **104-120** Burstein (1976)
Tibia **196.5**	**129** Meijer (2001) **196.5** Meijer (2001) modified **125** Bedewi (1998) **120-140** Burstein (1976)
Fibula **196.5**	**156** Meijer (2001) **196.5** Meijer (2001) modified
Talus **120**	
Calcaneus **120**	

Table B.4: yield stress of different bones as determined by different authors and as adopted for the model (left column)

Ligament	Ultimate load (N)	Ultimate strain (%)	Linear stiffness
anterior talofibular	**0-286** Parenteau (1996) [3] **67-193** Nigg (1990)	**24-44** Parenteau (1996) [3] **6-60** Nigg (1990)	**6-23 N/mm** Parenteau (1996) [3]
posterior talofibular	**307** Parenteau (1996) [3] **261.2** Attarian (1985)	**35** Parenteau (1996) [3] **100** Attarian (1985)	**37 N/mm** Parenteau (1996) [3]
calcaneofibular	**120-290** Parenteau (1996) [3] **265-327** Niggs (1990) **345.7** Attarian (1985) **29-87** Attarian (1985) cyclic load	**30-84** Parenteau (1996) [3] **27-81** Niggs (1990) **38** Attarian (1985)	**18-44 N/mm** Parenteau (1996) [3]
anterior tibiofibular	**138.9** Attarian (1985) **16-42** Attarian (1985) cyclic load	**53** Attarian (1985)	
posterior tibiofibular			
tibiocalcaneal			
anterior tibiotalar			
posterior tibiotalar			
plantar ligament	**238-506** Parenteau (1996) [3]	**12-32** Parenteau (1996) [3]	**39-495 N/mm** Parenteau (1996) [3]
talonavicular	**238.2-477.3** Davis (1996)	**35-87.4** Davis (1996)	**45.1-55.9 N/mm** Davis (1996) **9.0-10.2 N/mm^2** Davis (1996)
Achilles tendon	**1600-2000** Yamada (1970)		**982 N/mm** Hall (Dissertation) **2000±999 N/mm^2** Lewis (1997) ν = **0.4** Lewis (1997)

Table B.5: ligament and tendon mechanical properties as reported by different authors

Appendix C Geometry Properties

		Compact bone		Spongy bone	
Segment	Bone	Nr. nodes	Nr. elements	Nr. nodes	Nr. elements
Dist. Femur	Dist. Epiphys.	242	240	394	241
Tibia	Prox. Epiphys.	188	185	272	152
	Diaphysis	120	88		
	Dist. Epiphys.	158	158	195	102
Fibula	Prox. Epiphys.	55	56		
	Diaphysis	91	89		
	Dist. Epiphys.	45	47		
Talus	Talus	250	262		
Calcaneus	Calcaneus	232	239		
Tarsals	Cuboid	266	268		
	Navicular	219	224		
	Med. Cunei.	177	181		
	Int. Cunei.	222	232		
	Lat. Cunei.	147	152		
Metatarsals	Metatarsal 1	271	273		
	Metatarsal 2	165	166		
	Metatarsal 3	348	346		
	Metatarsal 4	466	470		
	Metatarsal 5	364	369		
Phalanxes	Prox. Phalan.1	290	288		
	Prox. Phalan.2	179	177		
	Prox. Phalan.3	392	390		
	Prox. Phalan.4	290	289		
	Prox. Phalan.5	264	266		
	Dist. Phalan.1	274	273		
	Dist. Phalan.2	81	79		
	Dist. Phalan.3	78	76		
	Dist. Phalan.4	143	141		
	Dist. Phalan.5	115	113		

Table C.1: Bone structure mesh properties

	Mass (g)	Centre of gravity w.r.t. heel origin (mm)			Moments of inertia (10^{-6} kg m^{-2})		
		x	y	z	I_{xx}	I_{yy}	I_{zz}
Tarsals	64.7	108	12	55	24.2	20.6	28.5
Metatarsals	125.5	149	-10	33	74.9	85.9	124.4
Phalanxes	46.2	201	23	27	26.9	9.8	32.7

Table C.2: Geometrical and inertial properties of the forefoot as calculated by a MADYMO subroutine

	Segment mass (g)	Weight Percentage Bone (%)	Bone Mass (g)	Other Tissue Mass (g)
Distal Femur	1500.0			
Proximal Tibia	**1855.8**			
Middle Tibia	**713.9**			
Distal Tibia	**315.0**			
Proximal Fibula			**36.2**	0.0
Middle Fibula			**27.2**	0.0
Distal Fibula			**8.4**	0.0
Talus	**70.9**	80	56.7	14.2
Calcaneus	**332.3**	60	199.4	132.9
Tarsals	**161.8**	40	64.7	97.1
Metatarsals	**313.8**	40	125.5	188.3
Phalanxes	**115.6**	40	46.2	69.4
Total	5379.1		564.4	501.8

Table C.3: Mass properties of mathematical human lower leg model. Boldfaced numbers are derived from [Hall, 1998]

Segment	Bone	Mass (g)	Density (kg m^{-3})	Element Thickness (mm)
Distal Femur	Dist. Epiphys. Cortical	619.0	2000	1.5
	Dist. Epiphys. Trabecular	193.8	1100	SOLID
Tibia	Prox. Epiphys. Cortical	708.1	20000	2.5
	Prox. Epiphys. Trabecular	1078.8	11000	SOLID
	Diaphysis	771.2	18000	2.5
	Dist. Epiphys. Cortical	242.6	12000	2.5
	Dist. Epiphys. Trabecular	206.5	6600	SOLID
Fibula	Prox. Epiphys.	33.5	6000	2
	Diaphysis	37.8	1500	2
	Dist. Epiphys.	9.1	1500	2
Talus	Talus	68.4	2000	3
Calcaneus	Calcaneus	128.3	4000	3
Total		4097.1		

Table C.4: Mass, density and geometry properties of bone mesh incorporated in finite element description

Appendix D UVa Test Setup

UVa experiment		3a	5c	5d	6i	7d
sex		female	female	female	male	male
age	[yr.]	67	62	59	67	51
specimen		left	right	right	right	left
height	[cm]	163	168	170	175	178
mass	[kg]	64	52	48	74	84
footpad thickness	[mm]	9.5	19.0	19.0	19.0	19.0
muscle pretens.		no	no	no	yes	yes
init. footpl. frc.	[N]	448	270	193	1340	920
init. kneepl. frc.	[N]	520	298	214	1893	1299
init. Achilles frc.	[N]	0	0	0	1024	1285
max. footpl. acc.	[g]	13.9	202	106	43	337
max. footpl. pos.	[mm]	22.6	78.6	80.7	8.9	75.1
max. tibia Fz	[N]	2204	3220	4800	4158	10836
injuries		none	calcaneus / tibial plateau	calcaneus / talus	none	lateral malleolus / pilon / tibial plateau

Table D.1: Overview of UVa experiments and their most apparent characteristics

UVa output parameters		
sensor	type	unit
footplate acceleration	acceleration	g
	velocity	m/s
	position	mm
footplate loadcell	Fx	N
	Fy	N
	Fz	N
	Mx	Nm
	My	Nm
knee plate loadcell	Fx	N
	Fy	N
	Fz	N
	Mx	Nm
	My	Nm
	Mz	Nm
femur load bolt	force	N
foot acceleration	x	g
	y	g
	z	g
tibia acceleration	x	g
	y	g
	z	g
ankle rotation	dorsiflexion / plantarflexion	°
	eversion / inversion	°
	internal / external rotation	°
tibia loadcell	Fx	N
	Fy	N
	Fz	N
	Mx	N
	My	N
	Tibia Index	-

Table D.2: Overview of UVa output parameters

Appendix E UVa Results

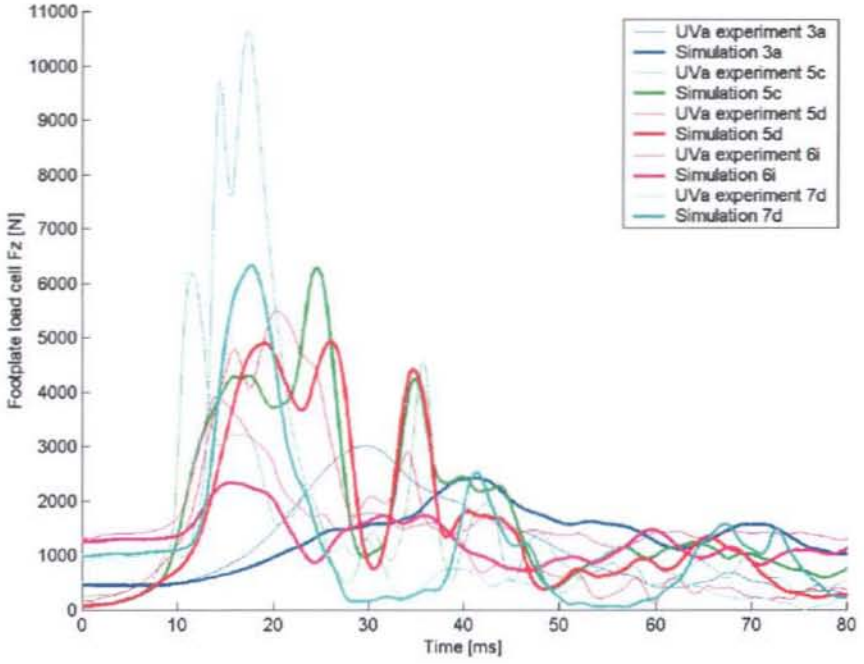

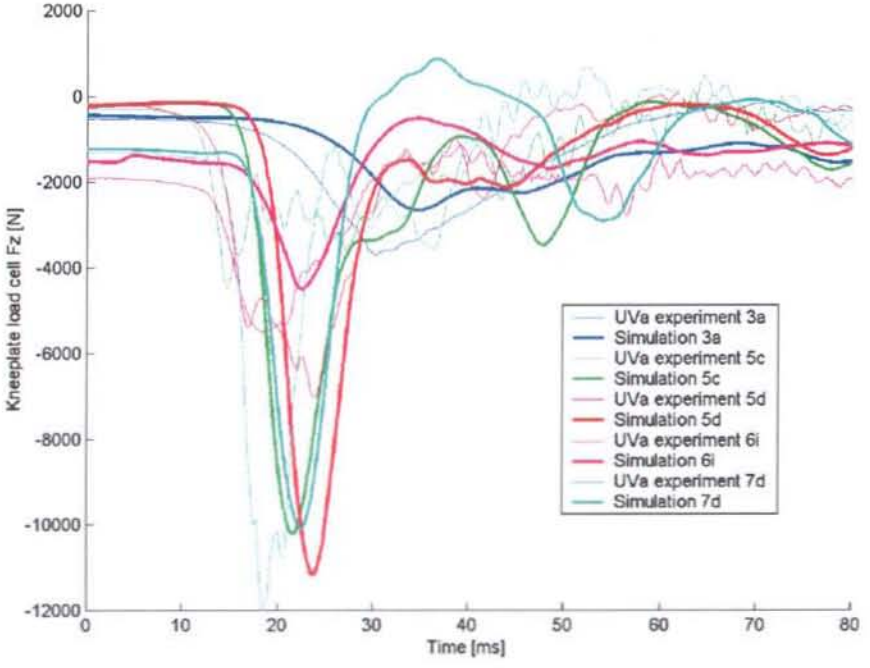

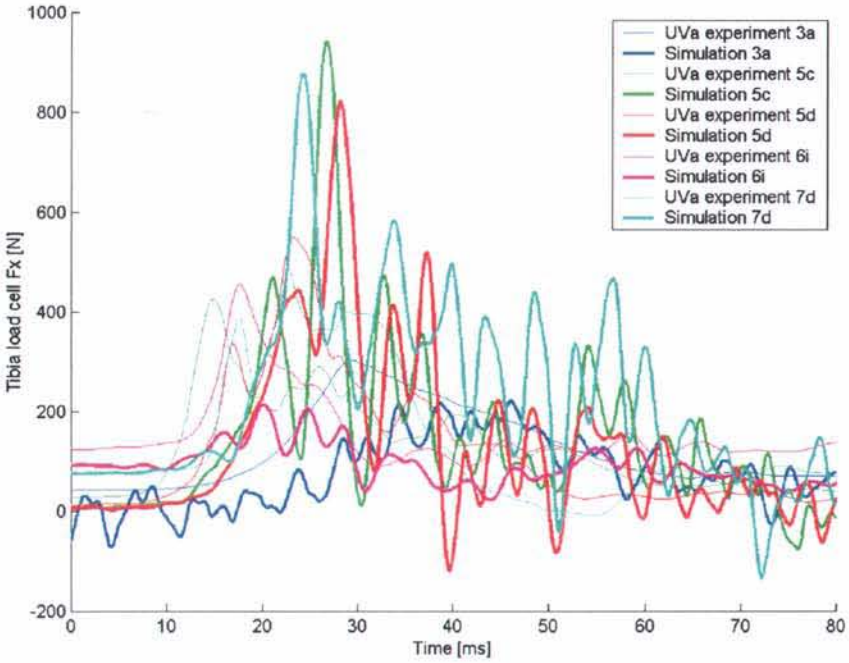
UVa experiment 3a
Simulation 3a
UVa experiment 5c
Simulation 5c
UVa experiment 5d
Simulation 5d
UVa experiment 6i
Simulation 6i
UVa experiment 7d
Simulation 7d
Tibia load cell Fx [N]
Time [ms]

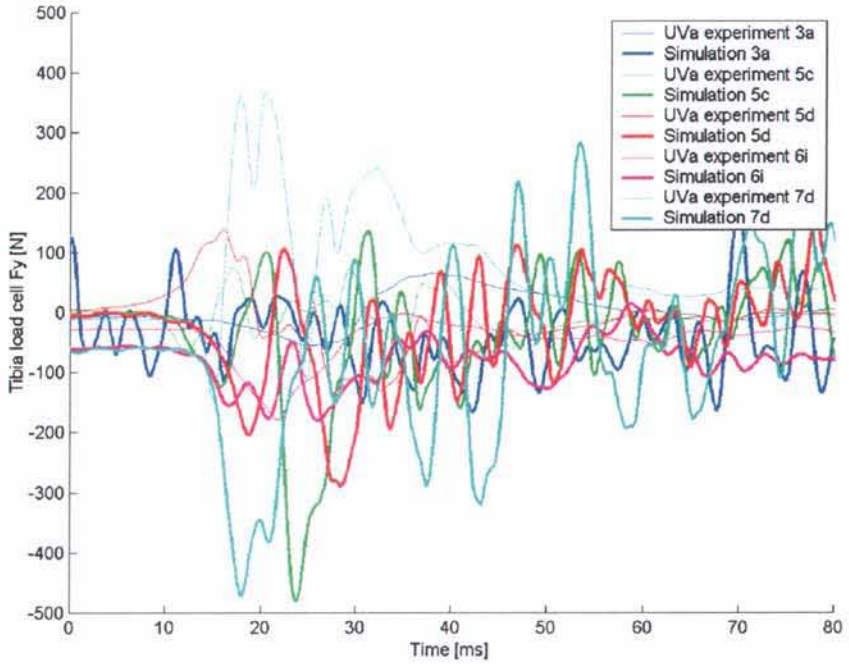
UVa experiment 3a
Simulation 3a
UVa experiment 5c
Simulation 5c
UVa experiment 5d
Simulation 5d
UVa experiment 6i
Simulation 6i
UVa experiment 7d
Simulation 7d
Tibia load cell Fy [N]
Time [ms]

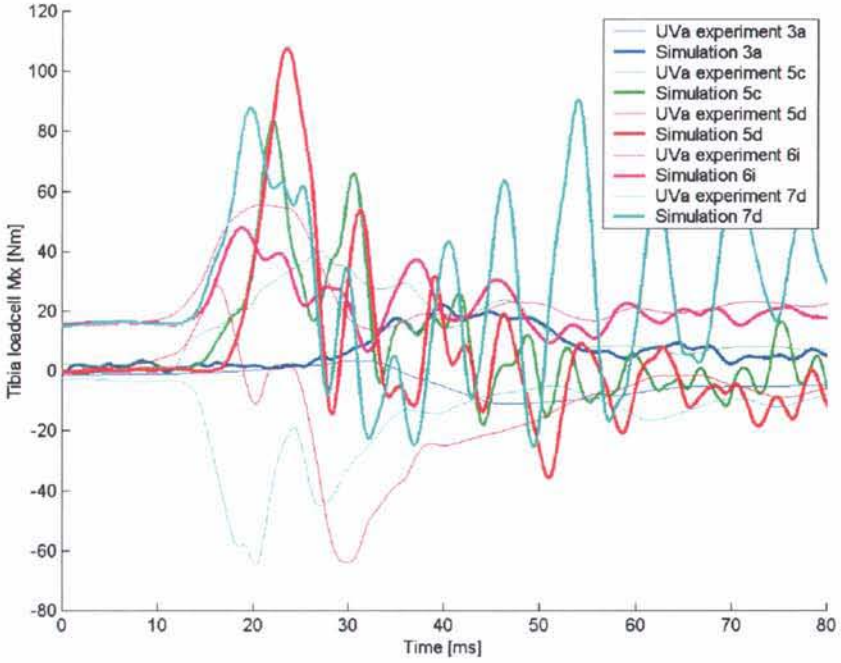
Tibia loadcell Mx [Nm]
Time [ms]
UVa experiment 3a
Simulation 3a
UVa experiment 5c
Simulation 5c
UVa experiment 5d
Simulation 5d
UVa experiment 6i
Simulation 6i
UVa experiment 7d
Simulation 7d

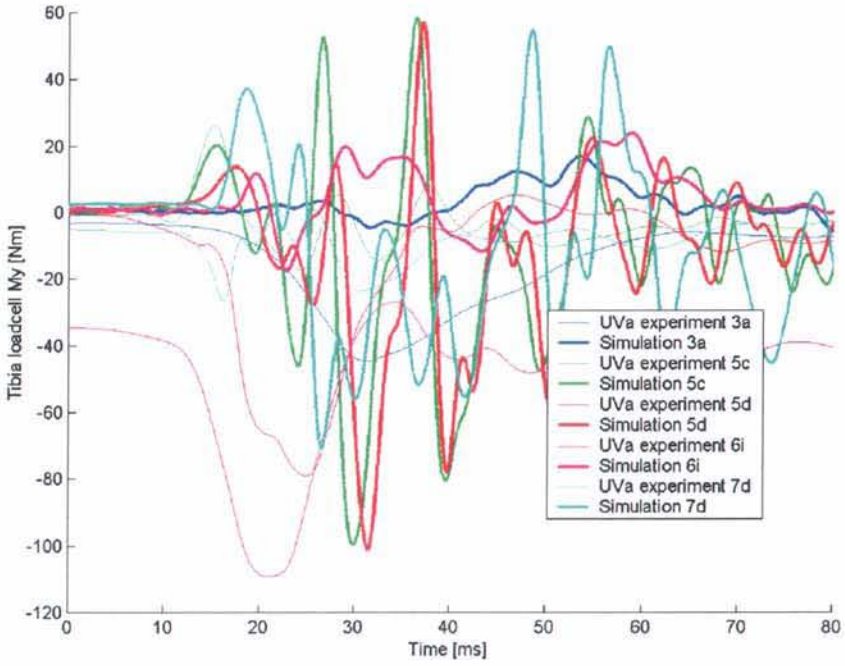
Tibia loadcell My [Nm]
Time [ms]
UVa experiment 3a
Simulation 3a
UVa experiment 5c
Simulation 5c
UVa experiment 5d
Simulation 5d
UVa experiment 6i
Simulation 6i
UVa experiment 7d
Simulation 7d

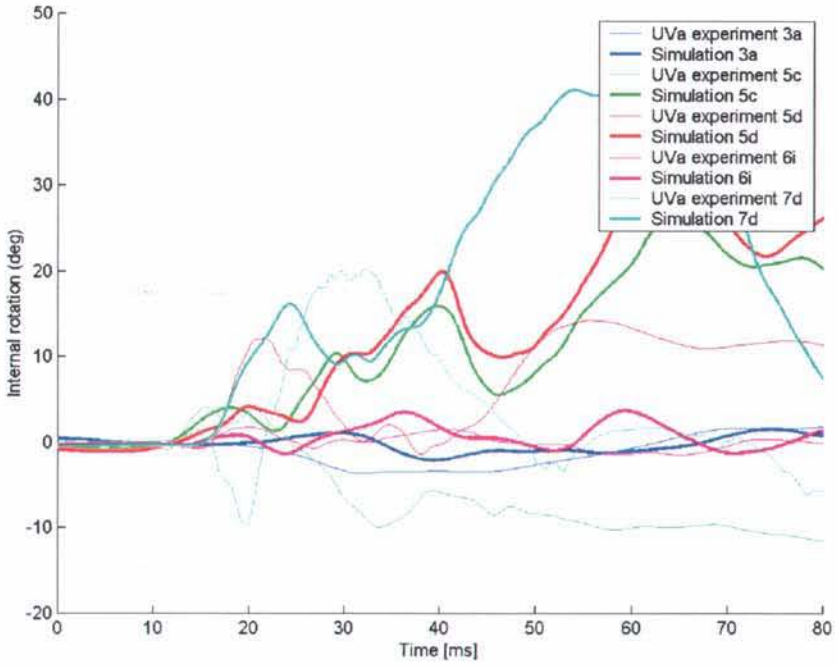
UVa experiment 3a
Simulation 3a
UVa experiment 5c
Simulation 5c
UVa experiment 5d
Simulation 5d
UVa experiment 6i
Simulation 6i
UVa experiment 7d
Simulation 7d
Internal rotation (deg)
Time [ms]
50
40
30
20
10
0
-10
-20
0
10
20
30
40
50
60
70
80

Appendix F TRL Results